PFC/JA-86-11

High Energy X-ray Measurements During Lower Hybrid Current Drive on the Alcator C Tokamak

S. Texter, S. Knowlton M. Porkolab, Y. Takase

Plasma Fusion Center
Massachusetts Institute of Technology
Cambridge, MA 02139

March 1986

This work was supported by the U.S. Department of Energy Contract No. DE-AC02-78ET51013. Reproduction, translation, publication, use and disposal, in whole or in part by or for the United States government is permitted.

High Energy X-ray Measurements During Lower Hybrid Current Drive on the Alcator C Tokamak

S. Texter, S. Knowlton, M. Porkolab, and Y. Takase

Plasma Fusion Center, Massachussets Institute of Technology,
Cambridge, Massachusetts, 02139

ABSTRACT

High energy x-ray emission ($E_\gamma > 20\,\mathrm{keV}$) from superthermal plasma electrons during lower hybrid current drive on the Alcator C tokamak has been measured using Sodium Iodide (NaI) scintillation spectroscopy. The x-ray spectra are generally linear on a semi-log plot of count rate vs. photon energy and extend out to several hundred keV. For the range of densities ($\bar{n}_e \approx 0.3 - 0.8 \times 10^{14}\,\mathrm{cm}^{-3}$) over which current drive was performed on Alcator, there was negligible emission before the injection of radiofrequency (rf) wave power. The radial profiles of the emission were also measured and indicate that the current carrying, high energy electrons exist primarily within the inner half ($r/a < 1/2$) of the plasma column. Plasma parameter scans produced variations in the x-ray emission profiles that are consistent with changes in the launched Fourier power spectrum, and the conditions imposed by lower hybrid wave accessibility. In addition, the velocity space distribution function of the energetic tail electrons has been determined using the angular variation in the x-ray emission.

I. Introduction

During lower hybrid current drive, an energetic, current carrying electron tail is created by the traveling radiofrequency (rf) waves [1]. This high energy tail emits a continuum of bremsstrahlung radiation due to collisions between the tail electrons and the bulk plasma ions. By measuring this emission, it is possible to diagnose these energetic electrons. To

this end, two different arrays of NaI spectrometers have been used to measure the hard x-ray ($E_\gamma > 20$ keV) emission during lower hybrid current drive on Alcator C. The first array measured the x-rays emitted perpendicular to the magnetic axis and was used to determine the radial profile of the emission. This emission indicates that the energetic electron tail extends out to several hundred keV, and is contained primarily within the inner half ($r/a < 1/2$) of the plasma column. There is negligible radiation before the injection of rf power. Parameter scans were performed by changing either the launched power spectrum, magnetic field, density, or toroidal plasma current. The observed variations in the x-ray emission were consistent with these parameter changes. In particular, variations in the plasma density and magnetic field directly affect the accessibility characteristics of the injected lower hybrid waves. The second array measured the x-ray emission as a function of the angle between the toroidal magnetic field and the emission direction. The emission is greatly enhanced in the forward (ohmic electron drift) direction, indicating a strong anisotropy of the electron distribution function. The data demonstrate the existence of a nearly flat parallel tail extending out to approximately 500 keV.

Similar measurements have been made on PLT and Versator [2,3]. However, the high frequency (f=4.6 GHz) and high rf powers (up to $\simeq$ 1 MW) used by Alcator C (major radius R = 64 cm, minor radius a = 16.5 cm) allowed us to make these measurements at comparatively high densities of up to $\bar{n}_e \simeq 0.8 \times 10^{14}\,\mathrm{cm}^{-3}$. The lower hybrid waves were launched by two 4 × 4 waveguide arrays located 180° relative to each other around the torus. As in past experiments [4], the primary winding of the ohmic heating transformer was open-circuited just before application of the rf power. Without rf power, the plasma current decays inductively with a typical time scale of $t_{L/R} \sim 150$ ms. Upon injection of sufficiently high rf power, the current decay is arrested and a constant current with zero loop voltage is maintained by the waves. In such cases, the vertical equilibrium magnetic field and the internal inductance reach a constant value within about 50 ms. Hence, after this transient time interval, inductive effects are negligible and the toroidal current is driven by the rf power alone. X-ray spectra are then collected for the remainder of the rf-current-driven phase of the discharge, approximately 150 ms in duration.

The plan of this paper is as follows: In Sec. II a brief discussion of the launched $n_{||}$ spectrum and lower hybrid wave accessibility is given, as it relates to the measurements shown in Sec. III. In Sec. III the perpendicular x-ray measurements are presented and discussed. The angular x-ray data is presented in Sec. IV, as well as the tail electron distribution function deduced from this data. Finally, a summary and conclusions are given in Section V.

II. LOWER HYBRID WAVE COUPLING AND ACCESSIBILITY

The theoretical $n_{||}$ "Brambilla" power spectrum [5] for the Alcator C waveguide array is shown in Fig. 1 [6]. The $n_{||}$ spectrum for 180° phasing (0-π-0-π) is peaking at $|n_{||}| = 3$ with most of the power between 2 and 4. Since this phasing is symmetric, the $n_{||}$ spectrum is symmetric in the positive and negative toroidal directions. The positive direction here is defined arbitrarily as the ohmic electron drift direction. Also shown is the power spectrum resulting from +90° phasing (0-$\frac{\pi}{2}$-π-$\frac{3\pi}{2}$). This is the phasing typically used during current drive experiments. In this case, most of the power is launched in the positive direction in the range $+1 < n_{||} < +2.5$. Note, however, that about 1/3 of the power is unavoidably launched in the negative direction and is centered near $n_{||} = -6$. The negative part of the spectrum is expected to be absorbed near the plasma surface [7].

The slow wave launching structure initially fixes the value of $n_{||}$ for a given wave packet. As the wave packet propagates inward toward the plasma center, its $n_{||}$ value can undergo changes due to toroidal effects [7], density fluctuations [8], the anomalous Doppler effect [9], or parametric decay [10]. However, for the plasma conditions under which current drive experiments were performed on Alcator, regardless of the wave packet's local $n_{||}$ value, the maximum extent of its penetration is determined by cold plasma lower hybrid theory from [11]

$$n_{\|} = \frac{\omega_{pe}}{\omega_{ce}} + \sqrt{1 + (\frac{\omega_{pe}}{\omega_{ce}})^2 - (\frac{\omega_{pi}}{\omega})^2}.$$

This condition defines a contour of accessibility inside of which a wave packet with a given value of $n_{\|}$ cannot penetrate. In general, a wave's accessibility improves with lower plasma density and larger magnetic field. Thus, the contours of accessibility are concentric circles (due to the plasma density) that are slightly distorted (due to the toroidal magnetic field). Figure 2 gives an example of these contours [12]. It is clear from the figure that waves with fast parallel phase velocities (low $n_{\|}$ values) are restricted to be further from the plasma center than slower waves. Therefore, the most energetic resonant electrons may not be generated at the plasma center, but at some distance radially outward. Furthermore, the collisional slowing down time of a fast electron increases with energy. Hence, fast electrons have more time to diffuse out of the plasma interior, whereas slower electrons are stopped there.

III. PERPENDICULAR X-RAY MEASUREMENTS

A. Experimental Setup

All the measurements described here were made by viewing the x-ray emission along chords through the plasma volume. The spectrometers were placed under the tokamak, viewing vertically upward, perpendicular to the horizontal midplane. A given set of measurements were always made with spectrometers at the same toroidal location viewing along parallel beamlines that formed a poloidal plane of intersection. The viewing beamlines were narrowly collimated with a diameter of about one centimeter.

Figure 3 shows a schematic diagram of the x-ray detector array used to collect the data discussed in this section. The array consisted of seven 2.54 cm $\times$ 7.62 cm NaI scintillation spectrometers. The instrument was designed to measure only direct plasma

bremsstrahlung. The reason for this was twofold. First, x-ray emission from any source other than the plasma does not directly indicate the real space or velocity space distribution of plasma electrons. Secondly, the major sources of non-plasma emission were the vacuum vessel wall and the plasma limiter, and this type of emission, called "thick target bremsstrahlung", is difficult to theoretically model. To prevent non-plasma x-radiation from entering the crystals and distorting the measured plasma signal, the entire array was placed inside a lead shield roughly 24 centimeters thick. Also, the viewing lines were tightly collimated to see only the plasma column. The vacuum window was made of 0.25 cm thick aluminum and was mounted on the outside of an Alcator port. This window permitted the unattenuated detection of photons with energies greater than 10 keV, while preventing non-plasma radiation from scattering into a collimator. The window was mounted approximately 45 cm from the plasma surface at the end of a viewing slot. This further prevented limiter and wall radiation from striking the vacuum window. Similarly, the viewing lines looked into a port on the top of Alcator which thereby functioned as a "black" beamdump. The array was also placed inside a magnetic shield roughly 3 cm thick. This shield prevented the penetration of the poloidal field into the photomultiplier tubes on the x-ray detectors, which would have distorted the measured signal.

Each detector of the array collected an x-ray energy spectrum. The spectra are generally linear on a semi-log plot of count rate vs. x-ray energy and extend out to several hundred keV. The spectra effective "temperature" (defined here as the mean photon energy of the spectral distribution) are in the range of several tens of keV. Each detector views emission from a particular chordal (radial) position in the plasma ranging from -12.4 cm to 9.4 cm. In general, each spectrum required several plasma shots (4 to 15) to achieve adequate statistical resolution at the high energy end. The crystals used in the detectors were large enough such that over the entire range of measured x-radiation (20-500 keV), no secondary scattered photons escaped. Thus, any incident photon deposited its full energy in the detector crystal. (The photofraction was greater than 0.95.) In this way, no corrections had to be made to the raw data that would have resulted in greater uncertainties.

B. X-ray Spectra and Profile Measurements

Figure 4 shows the photon energy spectrum collected from the plasma center. Also shown is the high energy plasma x-ray emission during the discharge before the rf power was turned on. The emission before the rf power is seen to be negligible compared to the emission during the rf driven phase of the discharge. This is a common feature of the rf driven discharges in Alcator and shows that over the range of plasma densities for which current drive experiments were performed here, there is usually no pre-formed high energy runaway electron tail. For the plasma conditions given, the x-ray spectrum tail extends out to at least 500 keV. However, the smallest value of $n_{||}$ permitted in the plasma center by lower hybrid theory is $n_{||} = 1.2$. This corresponds to a resonant electron energy of 400 keV. The discrepancy is probably due to the fact that since the measurement is chord averaged, the entire plasma density profile is sampled. Because of lower densities further out radially, faster waves are permitted there, leading to values of resonant electron energy up to at least 800 keV. However, this does not imply that the spectra terminates due to the effects of accessibility. Indeed, the spectrum shows no indication that a cutoff has been reached, and in fact is actually turning slightly upward. This could be due to energetic electrons beyond the resonant quasi-linear plateau, the effects of a small residual electric field, or simply noise (which is comparable to the signal level at the highest measured photon energies). Many of the spectra shown in this section do not extend out to the accessibility limit prescribed by lower hybrid theory for their respective plasma conditions. The reason is that since the spectra fall off exponentially, experimental run time was often not available to collect complete spectra. This was particularly true when radial profiles were being measured.

Figure 5(a) shows line-averaged (brightness) spectra from three different radial positions. As mentioned above, the high energy tail portion of each spectrum (20 to 200 keV) is very linear, with a correletion coefficient greater than 0.90 and a fractional standard deviation of less than 20 percent in all cases. Therefore, each spectral tail can be characterized by an "x-ray temperature". Caution must be exercised in interpreting this x-ray

temperature in that, unlike the case of low energy x-ray emission (soft x-ray spectroscopy), the x-ray temperature here does not equal the mean energy of the emitting electrons. As a general rule, the true mean energy of the emitting electrons will be greater than the resulting x-ray spectrum temperature. The reason for this is that as electrons approach relativistic energies, the bremsstrahlung emission cross section exhibits complicated velocity space structure, tending to fall off with emitted photon energy even for monoenergetic electrons.

In spite of this limitation, the x-ray spectra temperature provides a very good relative measure of the mean energy of the emitting electrons. Namely, if two spectra are compared and one has a greater temperature than the other, then the electrons that resulted in the former spectrum are more energetic than the electrons that produced the latter spectrum. Figure 5(a) shows a linear least squares fit to the semi-log data for the three radial positions given. As mentioned above the fits are very good. It can be seen that the tail electrons, while fewer in number, become more energetic at larger plasma radii. This is a general feature of the data resulting directly from the accessibility effects illustrated in Fig. 2.

Because spectra are obtained for several radial positions, it is possible to extract x-ray emission profiles at each measured photon energy. Figure 5(a) has small vertical arrows indicating five photon energies at which emission profiles have been obtained. The profiles are shown in Fig. 5(b). The emission profile for a given photon energy does not directly show the profile of the electrons of the same energy. This is due to the fact that all electrons with energies greater than the given photon energy contribute to the emission, and that the emission is also proportional to the bulk electron density. However, the emission profiles do provide a good relative measure of the fast electron density profiles. Figure 5(b) shows that the emission profiles become broader with increasing photon energy. This indicates that the relative abundance of high energy electrons compared to low energy electrons is greater in the outer region of the plasma than in the inner region. This is a general feature of the data obtained during current drive experiments.

Although the x-ray emission profiles are generally symmetric about the plasma axis, there appears to to be a consistent enhancement of the emission from the inboard side of the tokamak. This effect becomes more pronounced at higher photon energies. There are several possible explanations for this behavior. One possibility relates to the magnetic topology of the tokamak. The current direction is such that the helical twist of the field lines forces the current carrying high energy electrons to be traveling slightly downward on the inboard side. The relativistic forward scattering of bremsstrahlung radiation could then lead to enhanced emission from the inside of the tokamak. (The bremsstrahlung radiation emission pattern from a relativistic electron is approximately a narrow cone oriented in the same direction as the electron motion with an angular spread which varies as $1/\gamma^3$.) [13] Another possible mechanism relates to the constancy of the magnetic moment, μ. Since the local magnetic field is larger on the inboard side of the tokamak than on the outboard side, the inboard electrons will have a slightly larger fraction of their total energy in the perpendicular direction than the outboard electrons. Again, because of the forward scattering of bremsstrahlung radiation, this could lead to enhanced emission from the inboard side.

As with the x-ray spectra temperature, the emission profile widths can be quantitatively characterized by fitting an analytic function to the profile data. Figure 6 shows emission profiles for two photon energies fitted with shifted gaussians. The fits for all cases are good with fractional standard deviation less than 30 percent. The results of Figure 6 indicate quantitatively that the emission profiles broaden with increasing photon energies.

C. Parametric Dependence of X-ray Measurements

The data in the previous section has been quantitatively characterized in two different ways. First, the x-ray temperature, which gives a relative measure of the mean emitting electron energy, has been extracted from the x-ray spectra for each radial position. Secondly, the emission profile width, which gives a relative measure of the profile width of the emitting electrons, has been extracted from the emission data for each photon energy.

Using these characterizations, the following two subsections illustrate the emission data dependency on relative waveguide phasing, plasma toroidal magnetic field, bulk plasma density, and plasma toroidal current.

1. X-ray Spectra

Figures 7(a)-7(d) show plots of the effective temperature of the perpendicular x-ray emission as a function of chord position (or equivalently, radius). The photon energy range of the spectra to which the temperatures were fitted is 20-200 keV. From all plots, the x-ray temperature clearly has a smaller value at the plasma center than at either the inside or outside radial positions. Within the experimental error (statistical), the shape of each plot is symmetric about the plasma axis. This behavior is a common feature of all the data which cover a broad range of rf wave and plasma parameters. The temperature at the plasma edge is typically 50-70 % larger than the temperature at the plasma center. This is roughly the same percentage difference that exists between the maximum resonant electron energies permitted in the plasma center ($\sim$ 350 keV) and periphery ($\sim$ 600 keV) by lower hybrid accessibility theory.

Figure 7(a) shows the x-ray temperatures for two different values of relative phasing of waveguides in the launching antenna. At each radial location the emitting electrons are more energetic in the case of 67.5° phasing than in the 135.0° case. Emission data taken only from the center for 67.5°, 90.0°, 112.5°, and 135.0° show the same behavior. Thus, it is clear that the mean energy of all rf produced tail electrons increases as the relative phasing of the launching antenna decreases. This is a direct reflection of the fact that in the 67.5° case, there is significantly more power in low $n_{||}$ waves of the launched power spectrum than in the 135° case, as can be seen from Fig. 1. This means that a greater fraction of the power is being damped on more energetic electrons. Thus, the measured x-ray spectra, which are reflective of the relative mean energy of the emitting electrons, "track" the launched rf power spectra.

Figures 7(b) and 7(c) show the x-ray temperature as a function of plasma radius for several different values of toroidal magnetic field and plasma line-averaged electron density, respectively. Figure 7(b) indicates that the emitting tail electrons become increasingly energetic at all radii within the plasma as the magnetic field is raised. This is due to the fact that for all else held constant, as the magnetic field is increased at a local point within the plasma, the minimum value of $n_{||}$ accessible to that point decreases. Hence, the maximum extent of the high energy tail, at a given point in the plasma, increases with increasing toroidal magnetic field. Similarly, Fig. 7(c) shows that the emitting tail electrons become more energetic as the electron density is lowered at all plasma radii. This is again a consequence of the fact that for lower density, waves with smaller values of $n_{||}$ are accessible to that position.

Finally, Fig. 7(d) shows a plot of the x-ray temperature versus plasma position for three different toroidal plasma currents. These plots indicate that the mean energy of the tail electrons increases with increasing plasma current. There is no simple explanation for this behavior, since plasma current does not directly affect lower hybrid wave accessibility. However, one possible explanation involves the relationship between plasma current and rf power. The amount of rf power required for current drive increases linearly with increasing plasma current [4]. Thus, as the plasma current is increased, the electron distribution function quasi-linear plateau may become flatter in velocity space due to the increase in the injected rf power. This effect, which has been observed in the numerical studies of current drive by Bonoli, et al., could lead to more energetic x-ray emission [14] .

2. Radial Profiles

Figures 8(a)-8(d) each show plots of the x-ray profile width of the perpendicular x-ray emission as a function of photon energy. The profile widths were obtained by fitting a gaussian to the emission data at photon energies of 40, 80, 120, 160, and 200 keV. From all plots, the x-ray profile width clearly increases with increasing photon energy. This behavior is again consistent with the fact that lower hybrid wave accessibility restricts

the fastest waves, and consequently the most energetic resonant electrons, to the plasma periphery.

Figure 8(a) shows the x-ray profile widths for two different values of relative phasing of waveguides in the launching antenna. At all photon energies, the x-ray emission profiles are more peaked in the case of 67.5° phasing than in the 135.0° case. Also, the relative difference in profile widths increases at higher photon energies. Thus, it is clear that the radial distribution of rf produced tail electrons becomes narrower as the relative phasing of the launching antenna is decreased. This result is consistent with the fact that the 135° power spectrum has a greater fraction of power in high $n_{||}$ waves than does the 90° power spectrum. These higher $n_{||}$ waves tend to damp further out from the plasma center where the electron temperature is lower. Thus, the tail electron profiles tend to be broader in the 135° case.

Figures 8(b) and 8(c) show the x-ray emission profile width as a function of photon energy for several different values of toroidal magnetic field and plasma line-averaged electron density, respectively. Figure 8(b) indicates that the emitting tail electrons have a narrower radial distribution at all energies as the magnetic field is raised. Similarly, Fig. 8(c) shows that the profile of the high energy tail electrons becomes more peaked at all energies as the electron density is lowered. The difference in profile widths is greater for higher photon energies in both cases. As the field is lowered, or the density raised, the minimum value of $n_{||}$ accessible to the plasma interior increases, and the mean energy of the electrons present in the plasma interior decreases. This profile broadening is particularly pronounced at higher photon energies. This is probably due to the fact that the higher energy electrons, which determine the emission of the most energetic photons, are the most significantly affected by accessibility. At the lowest values of emitted photon energy, the profile width changes, as a function of magnetic field or density, are significantly smaller.

Finally, Fig. 8(d) shows a plot of the x-ray emission profile width versus photon energy for three different toroidal plasma currents. These plots indicate that the radial

distribution of the tail electrons broadens with increasing plasma current. Again, there is no simple explanation for this behavior. Waveguide phasing effects, magnetic field effects, and density effects, as discussed above, are all directly related to properties of the launched wave spectrum or lower hybrid wave accessibility. This is not the case with effects associated with varying the plasma current. The reason is that the plasma current has no direct bearing on the rf wave accessibility. However, the plasma current can affect the rf ray propagation through the $q(r)$ profile (where $q(r) = B_T r / B_\theta(r) R$). Numerical ray tracing studies by Bonoli, et al. indicate that the rf wave power deposition profile broadens with decreasing $q(a)$ (toroidal effects) [14] . This broadening is due to greater variation in the poloidal mode number, m, experienced by a propagating wave packet for lower values of $q(a)$. The variation in m can cause large increases in $n_{||}$ leading to wave damping at larger plasma radii. This mechanism can be used to explain the broader x-ray emission profiles experimentally observed at larger plasma currents. It is also consistent with the observation that the measured x-ray emission profile width increases with decreasing magnetic field (decreasing $q(a)$), although for that case, the effects of accessibilty probably dominate.

V. ANGULAR X-RAY MEASUREMENTS

All of the above measurements have dealt with the real space distribution of the rf generated high energy electrons. Of equal importance to the understanding of the physics issues associated with current drive is the velocity space distribution of these electrons. To determine the high energy electron distribution function, $f(\vec{p})$, generated during lower hybrid current drive experiments on Alcator C, a series of spectroscopic x-ray measurements have been made. This technique, which has been successfully used on the PLT tokamak [2,15], has been described in detail elsewhere [13,16], so only a brief discussion is given here.

In general, the bremsstrahlung x-ray emission due to a distribution of energetic plasma electrons is a convolution integral of the distribution function with the bremsstrahlung

cross section. As mentioned Sec. III, the bremsstrahlung cross section becomes increasingly peaked in the direction of the velocity of the emitting electron as the energy of the electron increases [13]. Thus, high energy bremsstrahlung emission in a given direction, relative to a fixed direction (the magnetic axis), tends to be due primarily to electrons whose velocity is also in the given emission direction. By measuring the x-ray emission at various angles relative to the magnetic axis, the anisotropy of the tail electron distribution function can be inferred. These "angular" measurements were made with the detector array shown in Fig. 9. (Only a single detector is shown. Five such detectors, each with a different viewing angle, are stacked atop one another to make the array.) Due to the Alcator port construction, the detectors were only 5mm $\times$ 5mm in size and could only be surrounded by about 3 cm of tungsten collimation. This limited the maximum photon energy for which the x-ray spectra could be reliably measured to about 200 keV. Wall radiation, which could contaminate the measurements, was probably not a problem since the spectra from the 90° angular detector and the central channel detector of the vertical array were virtually identical for the same plasma conditions. Since the measured x-ray spectrum for each angle was chord averaged, in order to compare the level of emission from angle-to-angle, each spectrum had to be normalized to the effective chord length. The electron tail density profile needed to perform the normalization was assumed to have the same shape as the x-ray emission profile discussed in the previous section (for the same plasma conditions) [15].

As mentioned above, the success of this technique relies on the fact that the bremsstrahlung cross section forces a correlation between a direction in electron velocity space, and the x-ray emission direction in real space. However, the measured x-ray energy distribution is not the electron energy distribution. The reason for this is that photons of a given direction and energy, k, can still result from electrons moving in arbitrary direction and with any kinetic energy greater than k. Due to these difficulties, it is not possible to uniquely determine the electron distribution from the bremsstrahlung data. Instead, a relatively simple model electron distribution function must be assumed. The parameters of the model which give calculated bremsstrahlung that best matches the measured data

can then by determined by iteration. The resultant distribution function is obviously not unique, but it should be a close approximation to the true electron distribution, and therefore be able to emulate many of its essential features. The model distribution function used here is a "three temperature Maxwellian". The tail has a gaussian velocity space shape and is characterized by three fitted parameters; a forward parallel temperature, $T_{\|F}$, a perpendicular temperature $T_\perp$, and a backward temperature $T_{\|B}$. The terms forward and backward refer to the direction of propagation of the low $n_\|$ lower hybrid waves. A fourth fitted parameter, a cutoff of the Maxwellian in the forward direction, T_{max}, is used to simulate the results of detailed computer code calculations [14] . These calculations indicate that the high energy distribution function formed during lower hybrid current drive is a very flat parallel plateau extending out to a sharp cutoff determined by lower hybrid wave accessibility. The model distribution function shape is assumed to be independent of plasma radius. Clearly the results of the previous section indicate that this assumption is not strictly correct. However, the PLT results suggest that the error incurred in this assumption affect only the electrons with energy greater than the limit prescribed by accessibility at the plasma center. For the plasma conditions under which the measurements presented in this section were made, this energy is about 400 keV. A position dependent distribution model function would remove these most energetic electrons from the inner half ($r/a < 1/2$) of the plasma and confine them to the outer half. The tail properties of either model (stored energy, dissipated power, cyclotron emission) are virtually identical.

Figure 10(a) shows the calculated x-ray emission that best matches the measured data for waveguide phasing of 90°. A contour plot of the model electron distribution function that results in the calculated bremsstrahlung is also shown in Fig. 10(b). The parameters for this distribution are $T_{\|F} = 800\,\mathrm{keV}$, $T_{\|B} = T_\perp = 100\,\mathrm{keV}$, and $T_{max} = 600\,\mathrm{keV}$. Note that the model distribution function has an enhanced temperature in the forward (wave phase velocity) direction. The calculated bremsstrahlung duplicates the two main features of the data: (1) The general peaking of the emission in the forward ($\theta_\gamma > 90°$) direction, and (2) the slope of the x-ray spectrum at each viewing angle (i.e., the spacing between lines of constant-photon-energy emission).

The cutoff energy T_{max} was introduced to simulate the high energy limit on the distribution function that could result from a restriction imposed on the maximum wave phase velocity prescribed by the lower hybrid accessibility condition. However, it is not possible with the present data to clearly distinguish between models with a cutoff energy and those without. This is particularly true here where experimental conditions limited the maximum measured photon energy to about 200 keV. A best fit with $T_{max} \rightarrow \infty$ is obtained for $T_{\|f} = 500\,\mathrm{keV}$. In this case, the parallel forward temperature is somewhat decreased from the previous model to compensate for the increased number of high energy tail electrons. The parallel backward and perpendicular temperatures are not affected by the choice of T_{max} since they are so much smaller. In either case, there is clearly a large high energy electron tail extending preferentially in one toroidal direction. To distinguish between the two models, data from over 500 keV would be required.

For the plasma conditions under which the emission data of Fig. 10 were collected ($\bar{n}_e = 3 \times 10^{13}\,\mathrm{cm}^{-3}$, B=8T, Hydrogen gas, $I_p = 140\,\mathrm{kA}$), lower hybrid wave accessibility restricts resonant electron energies to below 400 keV at the plasma center. This value increases at larger radii due the decreased density and increased magnetic field. The cut-off value of $T_{max} = 600$ keV was chosen because it best fits the data. Also, it is not possible to fit the data with a smaller value. Thus, it must be concluded that the measured distribution function is actually the true distribution averaged over the plasma poloidal cross section. This is in keeping with the fact the the measurements are all chord averaged.

Figure 11(a) shows actual and fitted emission data for plasma conditions similar to those of Fig. 10(a), but with a waveguide phasing of 135°. The model distribution used to fit the data is shown in Fig. 11(b). The general features of the distribution function here are similar to the 90° case, except that the temperatures of the distribution are significantly reduced to $T_{\|F} = 200\,\mathrm{keV}$, and $T_{\|B} = T_\perp = 70$ keV. The cutoff energy was kept at T_{max} = 600 keV since the plasma conditions, which determine accessibility, are unchanged. The depreciation of the temperatures is particular sever for the forward parallel temperature. As in the previous section, this is due to the difference in the shape of the launched

Fourier power spectrum. Figure 1 shows that there is much more power at low values of $n_{||}$ (corresponding to high phase velocity waves) in the 90° case than in the 135° case. This is reflected in the slope of the distribution function. In particular, for 90° phasing the power in the launched Fourier spectrum increases monotonically as $n_{||}$ decreases from 3 to 1. This corresponds to resonant electron kinetic energies ranging from 30 keV to that prescribed by accessibility. For the 135° case, the power spectrum peaks at about $n_{||} = 2$ ($\approx$ 100 keV), and extends from $n_{||} = 4$ down to the accessibility limit. For $T_{max} \rightarrow \infty$, $T_{||F}$, $T_{||B}$, and $T_{\perp}$ are unchanged. The reason is that in the 135° case, $T_{max} \gg T_{||F}$, so that the shape of $f(\vec{p})$ is determined only by the launched rf power spectrum and not accessibilty. Thus, the exact value of T_{max} has little effect on the calculated emission.

V. Summary and Conclusions

Perpendicularly emitted plasma hard x-ray spectra ($E_\gamma > 20\,\mathrm{keV}$) have been collected from Alcator C during purely lower hybrid current driven discharges at seven different chordal (radial) locations. The spectra were linear on a semi-log scale, extended out to several hundred keV, and had effective "temperatures" (again, defined here as the mean photon energy of a spectral distribution of photons) of several tens of keV. There is negligible emission before the rf power is turned on and the emission profiles are generally radially peaked, existing primarily within the inner half ($r/a < 1/2$) of the plasma column. The data was characterized by displaying, (a) the temperature of the spectra for each radial position, and (b) the width of the emission profile for each photon energy. For all the data presented, the temperature of the spectra increases with plasma radius. Equivalently, the emission profiles are broader at higher photon energy. The reason for this is believed to be the fact that the plasma density is lower at larger radii so that waves with correspondingly lower minimum values of $n_{||}$ are accessible there. Thus, the mean tail electron energy increases with plasma radius and this is reflected in the x-ray emission.

Scans of waveguide phasing, magnetic field, density, and current have been carried out.

The temperatures of the spectra at all positions were found to increase with decreasing waveguide phasing, increasing magnetic field, decreasing density, and increasing current. The "hardening" of the spectra with decreasing phasing is due to the greater fraction of power concentrated in the low $n_{||}$ waves of the launched Fourier spectrum. That is, the x-ray spectra "track" the launched power spectrum (at least at high energies, i.e., low values of $n_{||} \leq 3$). The hardening of the x-ray spectra with increasing magnetic field and decreasing density is directly related to wave accessibility. For a given plasma position, as the field is raised or the density lowered, the minimum value of $n_{||}$ with which waves can penetrate decreases. Thus, the mean energy of electrons, and hence the emitted x-ray spectrum temperature, increases at each position. The temperatures of the x-ray spectra increase with plasma current at all plasma radii. This is not a consequence of accessibility but may simply result from the fact that more rf power is required to produce steady state current drive as the amount of current being driven is raised. As the power is raised, the quasi-linear electron tail becomes flatter. This can result in a more energetic x-ray spectrum.

The x-ray emission profile widths were also presented as a function of waveguide phasing, magnetic field, density, and current. The emission profiles broaden with increasing waveguide phasing. This is consistent with the fact that high $n_{||}$ waves, which are more prevalent at larger values of waveguide phasing, tend to damp further out from the plasma center where the electron temperature is lower. The emission profiles broaden as the magnetic field is lowered or the density raised. The effect is particularly pronounced for the highest photon energies. As the field is lowered, or the density raised, accessibility increasingly restricts low $n_{||}$ waves from the plasma interior. The resulting average tail electron energy there is lowered, and this can give rise to broader emission profiles. The emission profiles broaden as the plasma current is raised. The decreased $q(a)$ tends to give larger upshifts in $n_{||}$ which can lead to broadening of the wave power deposition profile. A similar effect occurs as the magnetic field is lowered, but accessibility, which determines the location of the center of power deposition, probably dominates.

The x-ray emission measured as a function of the angle between the magnetic axis and the emission angle has been used to reconstruct distribution function of the high energy tail electrons. The tail distribution function was found to be highly anisotropic with a forward temperature about eight times larger than the perpendicular or backward temperatures. The distribution function was found to "track" with the launched rf power spectrum in the same manner as the perpendicular x-ray emission.

Finally, we note that the present experiments give little information on the low and intermediate energy electrons (i.e., electrons with energies in the range $E_\gamma \leq 30\,\mathrm{keV}$ which resonate with waves having $n_{||} > 3$). That is the regime where little or no rf power is launched, yet large numbers of electrons must exist to feed the high energy tail population. In particular, this is the regime of the so-called "spectral gap", where some mechanism must exist to upshift a significant part of the launched wave spectrum to diffuse electrons from the bulk. Unfortunately, the soft x-ray emission is dominated by the high energy electrons, and therefore quantitative information on low energy energy electrons is difficult to obtain.

We gratefully acknowledge the assistance of the Alcator physics and technical staff, Mr. Dave Griffin and his technical staff for their tireless maintainance of the rf system, and especially Dr. Paul Bonoli for his collaboration on many of the physics issues of this paper.

REFERENCES

[1] FISCH, N. J., Phys Rev. Lett. **41** (1978) 873; KARNEY, C. F. F., FISCH, N. J., Phys. Fluids **22** (1979) 1817.

[2] VON GOELER, S. *et al.*, Nucl. Fusion **25** (1985) 1515.

[3] MAYBERRY, M. J., *et al.*, Bull. Am. Phys. Soc. **28** (1983) 1031.

[4] PORKOLAB, M., *et al.*, Phys. Rev. Lett. **53** (1984) 450.

[5] BRAMBILLA, M., Nucl. Fusion **16** (1976) 47.

[6] PORKOLAB, M., (Proc. of the Fifth Top. Conf. on Radio Frequency Plasma Heating), invited paper B.1, p. 88, Madison, Wis., 1983.

[7] BONOLI, P. T., ENGLADE, R., (Proc. of the Fifth Top. Conf. on Radio Frequency Plasma Heating), paper A-L.1, p. 72, Madison, Wis., 1983.

[8] BONOLI, P. T., OTT, E., Phys. Fluids **25** (1982) 359.

[9] LIU, C. S., CHAN, V., BHADRA, D., HARVEY, R.,Phys. Rev. Lett. **48** (1982) 1479.

[10] TAKASE, Y., *et al.*, Phys. Fluids **28** (1985) 983; TAKASE, Y., *et al.*, Phys. Rev. Lett. **53** (1984) 274.

[11] STIX, T. H., **The Theory of Plasma Waves** (McGraw-Hill, Inc., New York, 1962); PORKOLAB, M., in **Fusion**, Ed. E. Teller, (Academic Press, New York, 1981) Vol. 1B, p. 165.

[12] LLOYD, B., *et al.*, *IAEA Technical Committee Meeting on Non-Inductive Current Drive in Tokamaks*, p. 250, Culham, England, 1983.

[13] GLUCKSTERN, R. L., HULL, M. H., Phys. Rev. **90** (1953) 1030; VON GOELER, S., *et al.*, Princeton Plasma Physics Laboratory, Reports PPPL-2010 and PPPL-2012 (1983).

[14] BONOLI, P. T., ENGLADE, R., PORKOLAB, M., in Heating in Toroidal Plasmas (Proc. 4th Int. Symp.) editors H. Knoepfel and E. Sindoni, (International School of Plasma Physics, EUR-9341-EN, 1984) Vol. II, p. 1311.

[15] STEVENS, J., *et al.*, Nuclear Fusion **25** (1985) 1529.

[16] TEXTER, S., Plasma Fusion Center, M.I.T., Report PFC/RR-85-24 (1986).

FIGURE CAPTIONS

Fig. 1. - The Brambilla[5] $n_{||}$ Fourier power spectrum for the Alcator C Waveguide array for different phasings $\Delta\phi$ between adjacent waveguides (after ref. 6) and the corresponding resonant electron energy.

Fig. 2. - Contours of accessibility in the poloidal plane of Alcator for given values of $n_{||}$ (after ref. 12). For a given $n_{||}$, the wave can propagate in the region outside the dashed contour. The plasma parameters are: Parabola-to-1/2 power density profile with a line averaged density of $\bar{n}_e = 5.5 \times 10^{13}\,\mathrm{cm}^{-3}$, B = 10 T on axis, Hydrogen.

Fig. 3. - Schematic diagram of the NaI scintillator array used to collect x-ray spectra emitted perpendicular to the magnetic axis. The detector crystals are 2.54 cm $\times$ 7.62 cm ($1'' \times 3''$) in size, and the vacuum window is 0.25 cm (0.010″) thick.

Fig. 4 - Central chord x-ray spectra emitted perpendicular to the magnetic axis during a purely rf driven discharge with and without rf power.

Fig. 5 - (a) Perpendicularly emitted x-ray spectra from three chordal locations. (b) Perpendicular x-ray brightness profiles for five photon energies.

Fig. 6 - The brightness profiles shown in Fig. 5(b) fitted with gaussian curves. The energies and profile widths are (a) 40 keV with a 1/e width of 7.4 cm and (b) 120 keV with a 1/e width of 8.6 cm.

Fig. 7 - Perpendicular x-ray spectra slope (effective x-ray "temperature") as a function of the collecting detector position parametrically in (a) waveguide phasing, (b) toroidal magnetic field, (c) line-averaged plasma density, and (d) toroidal

plasma current.

Fig. 8 - Perpendicular x-ray profile widths as a function of the collecting detector position parametrically in (a) waveguide phasing, (b) toroidal magnetic field, (c) line-averaged plasma density, and (d) toroidal plasma current.

Fig. 9 - Schematic diagram showing the top view of the "angular" x-ray detector array. (Only a single detector is shown. The array consists of five detectors, each viewing the plasma at a different angle, stacked atop one another.)

Fig. 10 - (a) X-ray emission for a waveguide phasing of 90°. The symbols are the measured data and the solid lines are the emission calculated from the model distribution function shown in (b). (b) Contour plot of the model tail electron distribution function.

Fig. 11 - (a) X-ray emission for a waveguide phasing of 135°. The symbols are the measured data and the solid lines are the emission calculated from the model distribution function shown in (b). (b) Contour plot of the model tail electron distribution function.

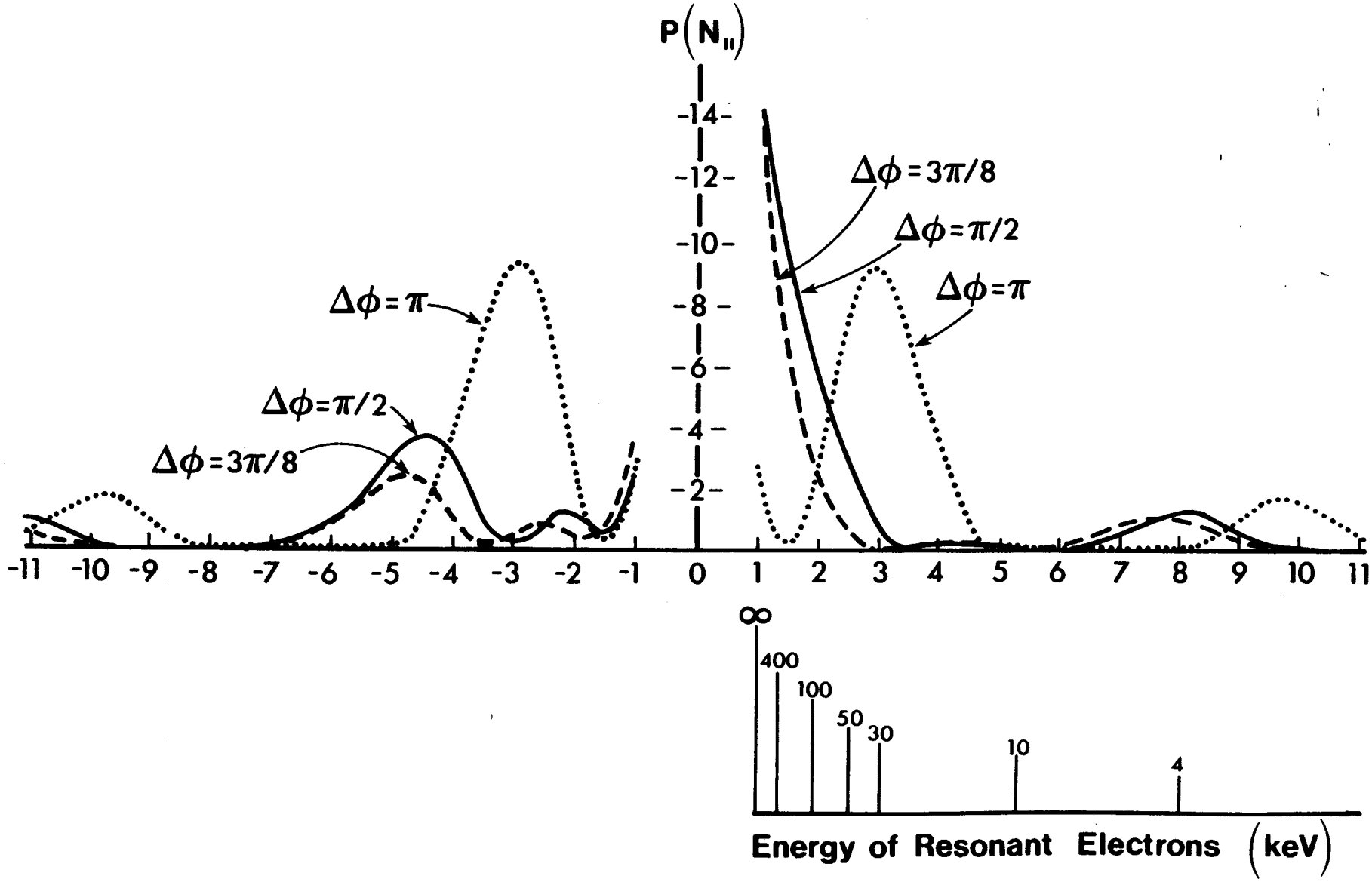
P(N∥)
-14-
-12-
-10-
-8-
-6-
-4-
-2-
Δφ=3π/8
Δφ=π/2
Δφ=π
Δφ=π
Δφ=π/2
Δφ=3π/8
-11 -10 -9 -8 -7 -6 -5 -4 -3 -2 -1 0 1 2 3 4 5 6 7 8 9 10 11
∞
400
100
50
30
10
4
Energy of Resonant Electrons (keV)

Figure 1

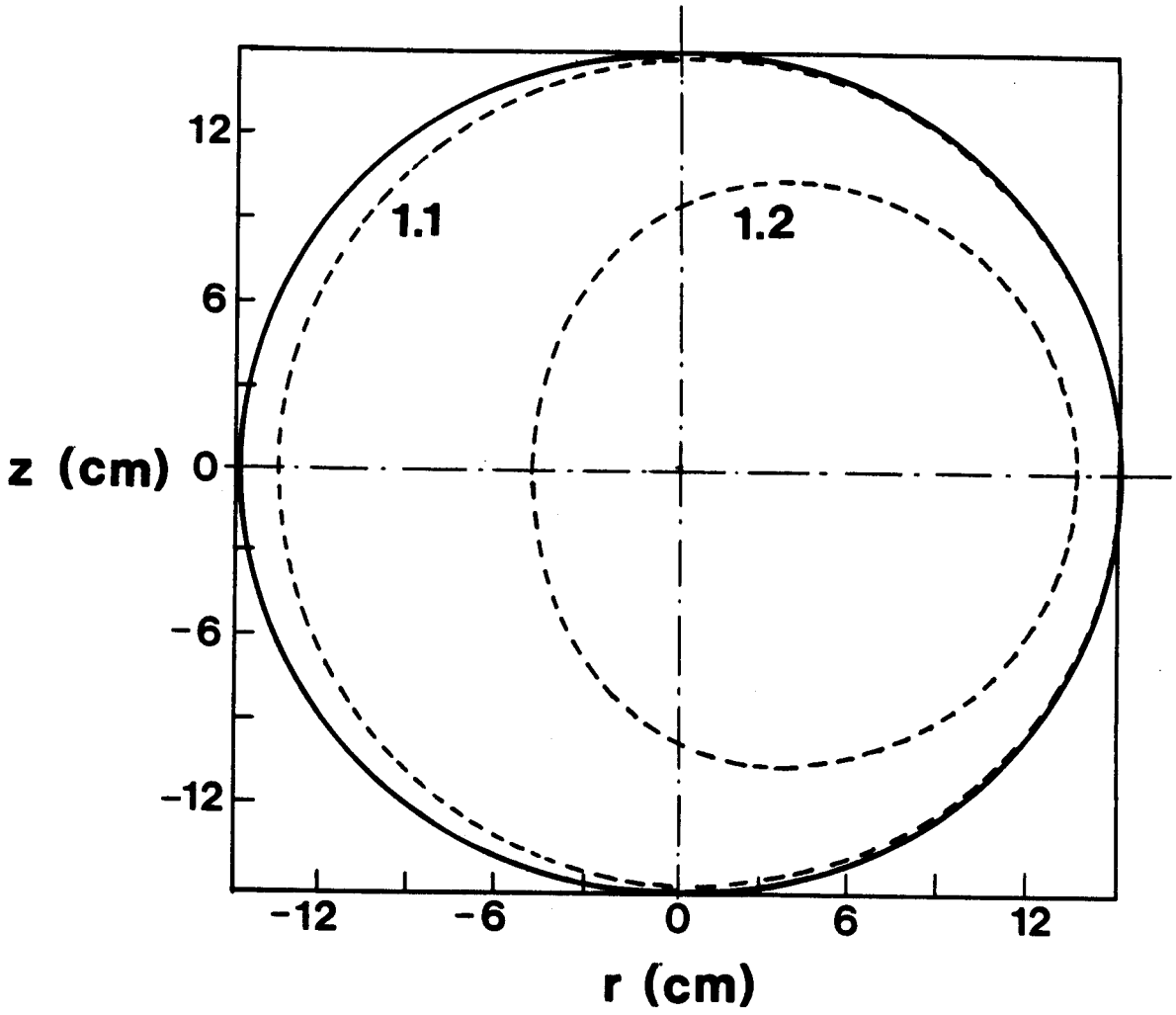

Figure 2

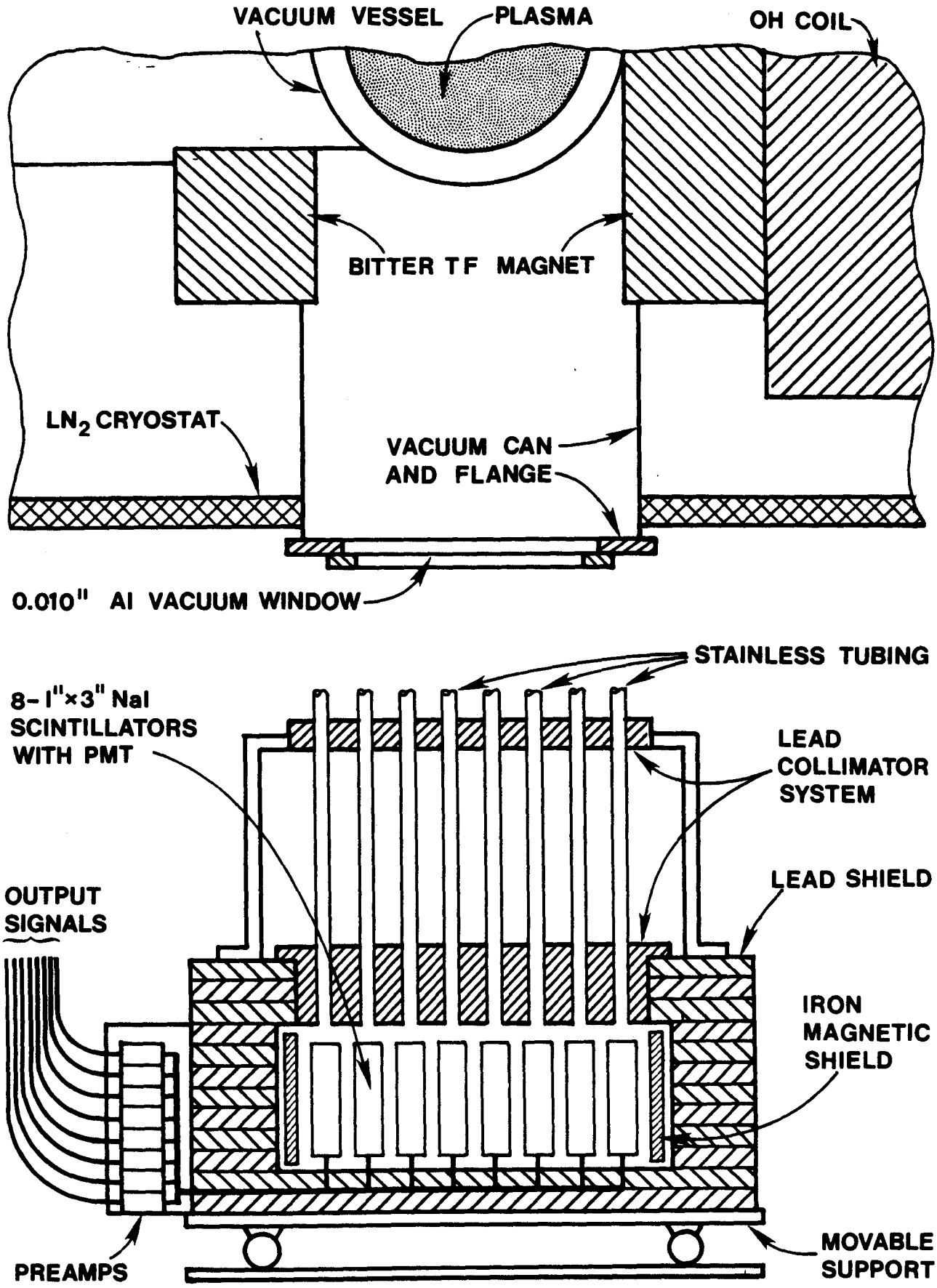
VACUUM VESSEL
PLASMA
OH COIL
BITTER TF MAGNET
LN2 CRYOSTAT
VACUUM CAN
AND FLANGE
0.010" Al VACUUM WINDOW
STAINLESS TUBING
8-1"×3" NaI
SCINTILLATORS
WITH PMT
LEAD
COLLIMATOR
SYSTEM
LEAD SHIELD
OUTPUT
SIGNALS
IRON
MAGNETIC
SHIELD
PREAMPS
MOVABLE
SUPPORT

Figure 3

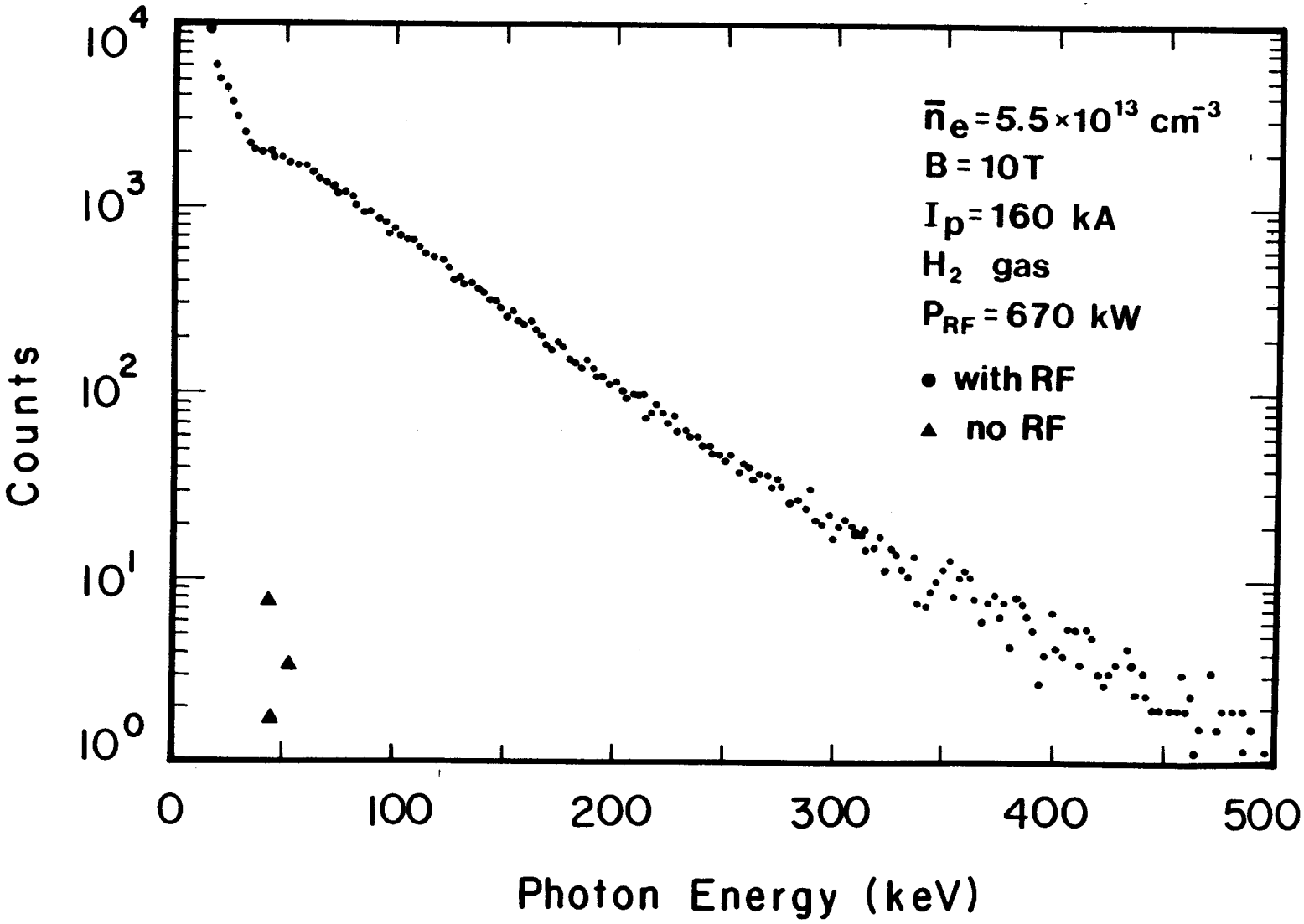
10^4
10^3
10^2
10^1
10^0
Counts
$\bar{n}_e = 5.5 \times 10^{13}$ cm^{-3}
B = 10T
I_p = 160 kA
H_2 gas
P_{RF} = 670 kW
• with RF
▲ no RF
0
100
200
300
400
500
Photon Energy (keV)

Figure 4

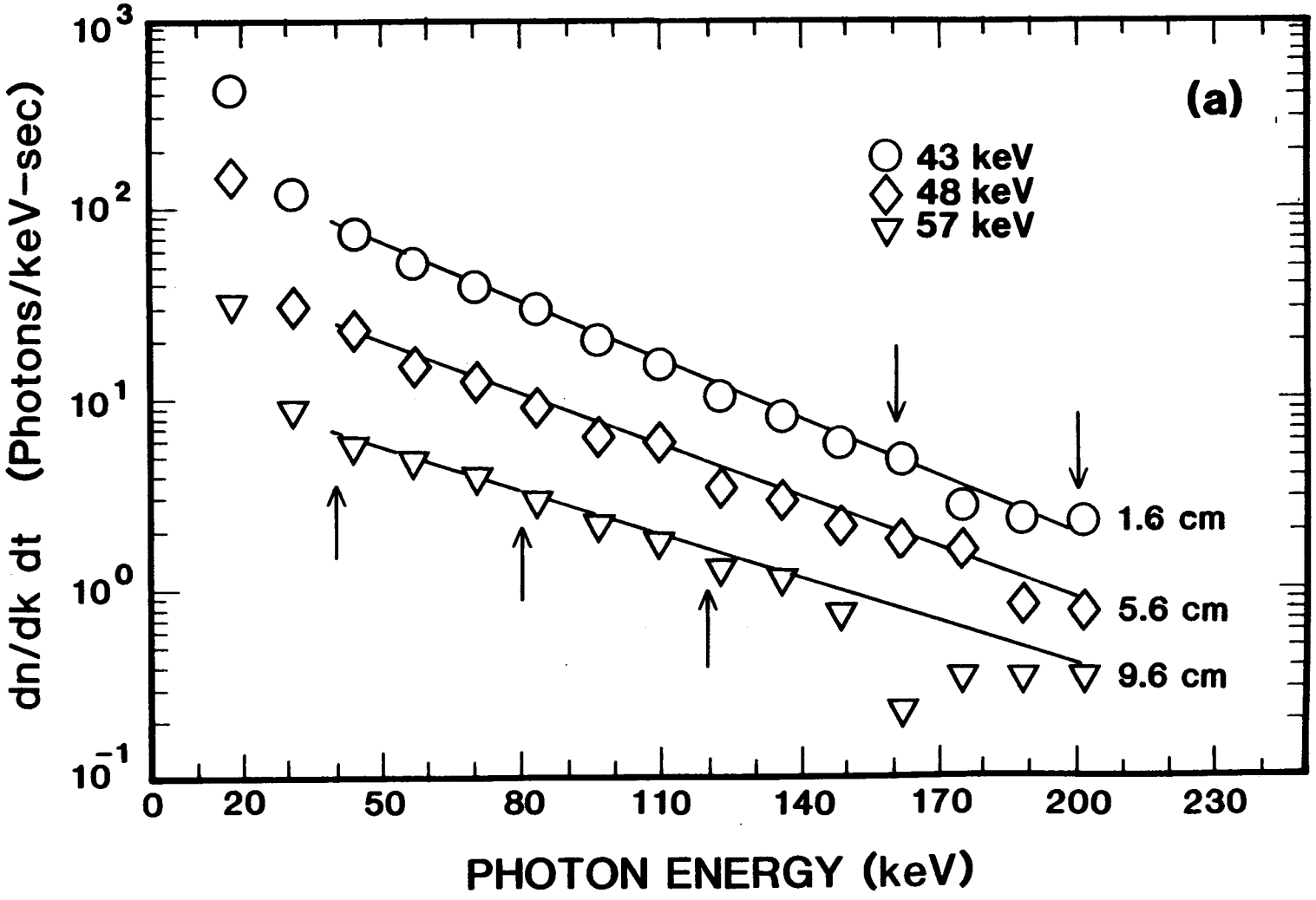
(a)
43 keV
48 keV
57 keV
1.6 cm
5.6 cm
9.6 cm
dn/dk dt (Photons/keV-sec)
10^3
10^2
10^1
10^0
10^{-1}
0
20
50
80
110
140
170
200
230
PHOTON ENERGY (keV)

Figure 5 (a)

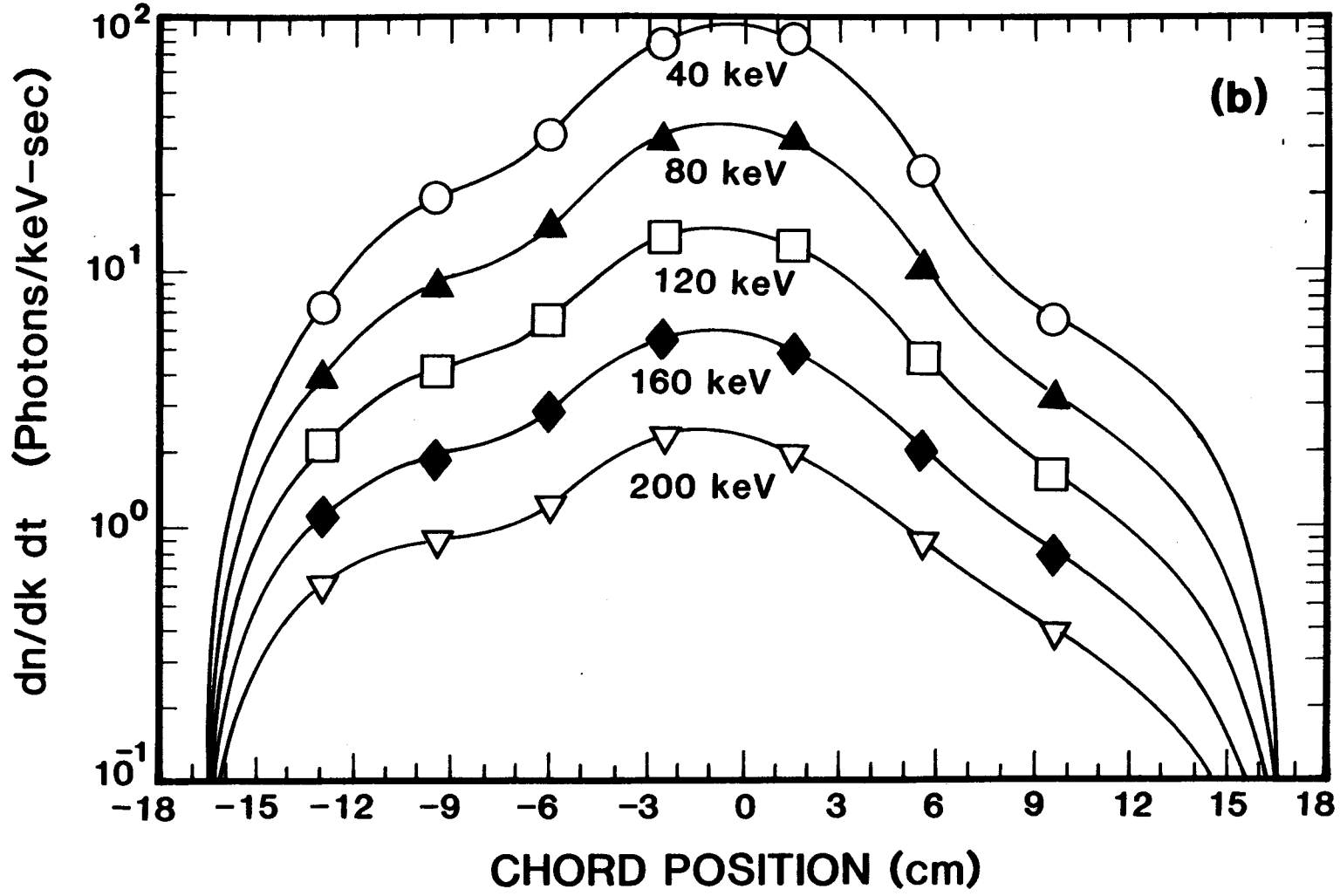
(b)
40 keV
80 keV
120 keV
160 keV
200 keV
dn/dk dt (Photons/keV-sec)
10^2
10^1
10^0
10^{-1}
-18 -15 -12 -9 -6 -3 0 3 6 9 12 15 18
CHORD POSITION (cm)

Figure 5 (b)

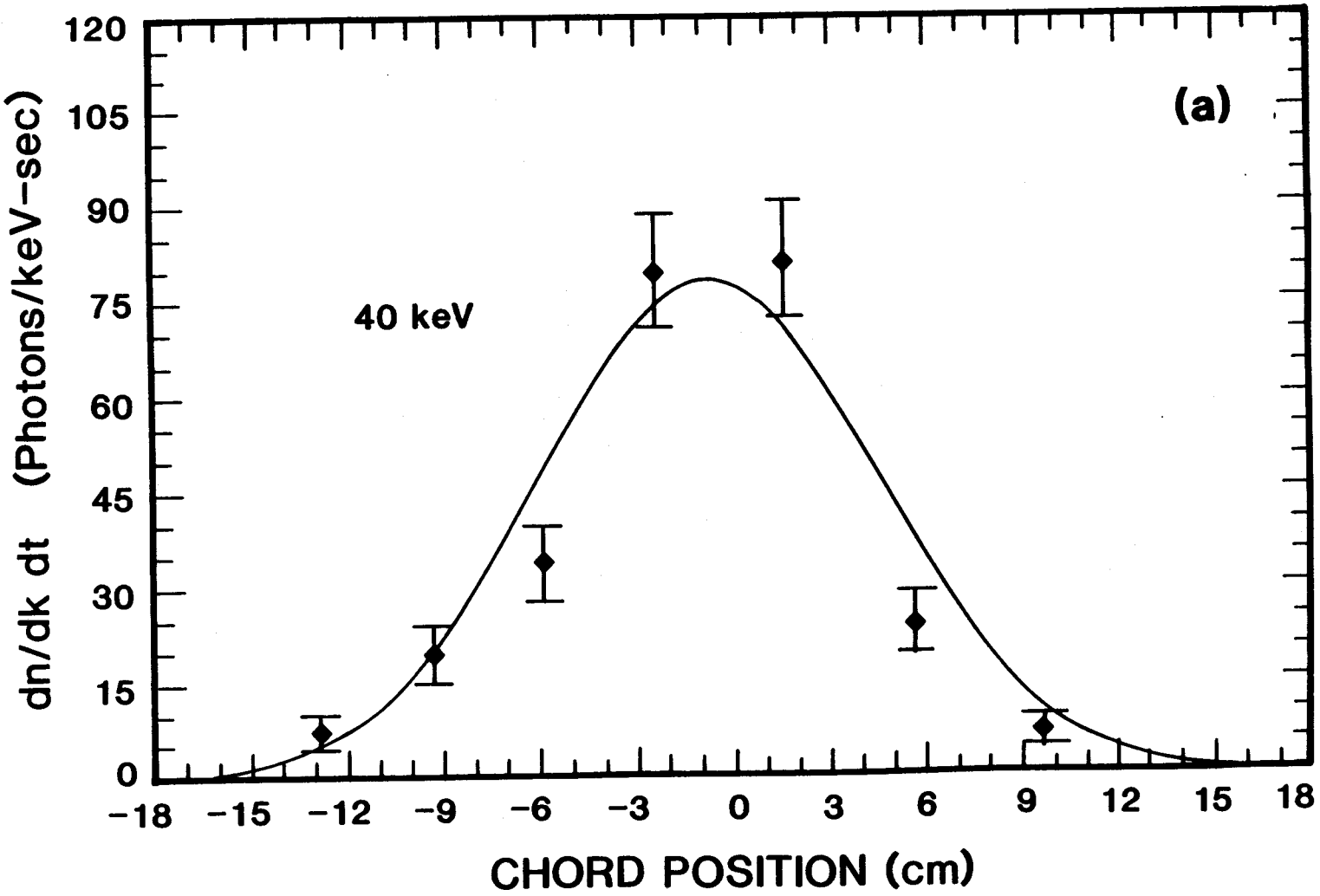
(a)
40 keV
dn/dk dt (Photons/keV-sec)
120
105
90
75
60
45
30
15
0
-18
-15
-12
-9
-6
-3
0
3
6
9
12
15
18
CHORD POSITION (cm)

Figure 6 (a)

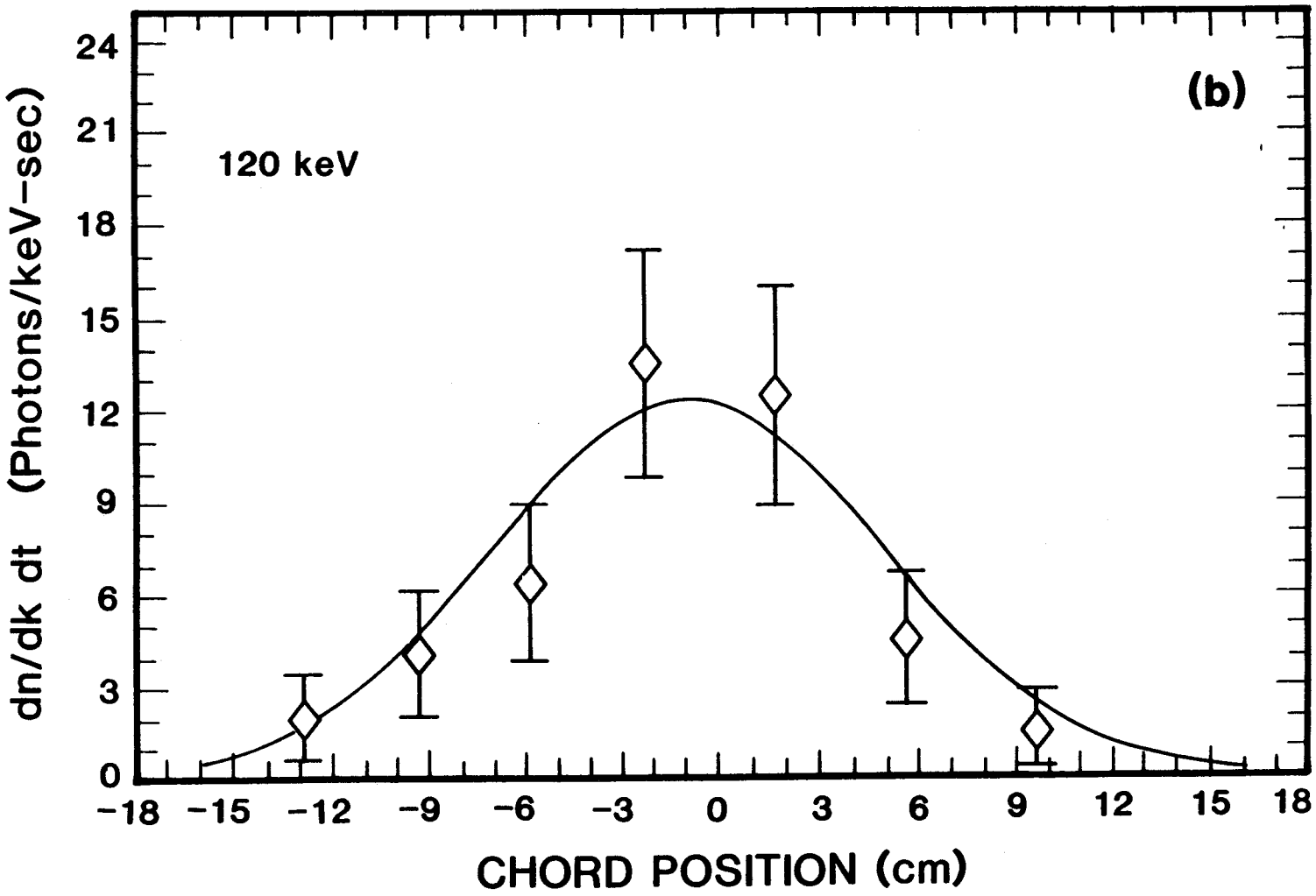
(b)
120 keV
dn/dk dt (Photons/keV-sec)
24
21
18
15
12
9
6
3
0
-18 -15 -12 -9 -6 -3 0 3 6 9 12 15 18
CHORD POSITION (cm)

Figure 6 (b)

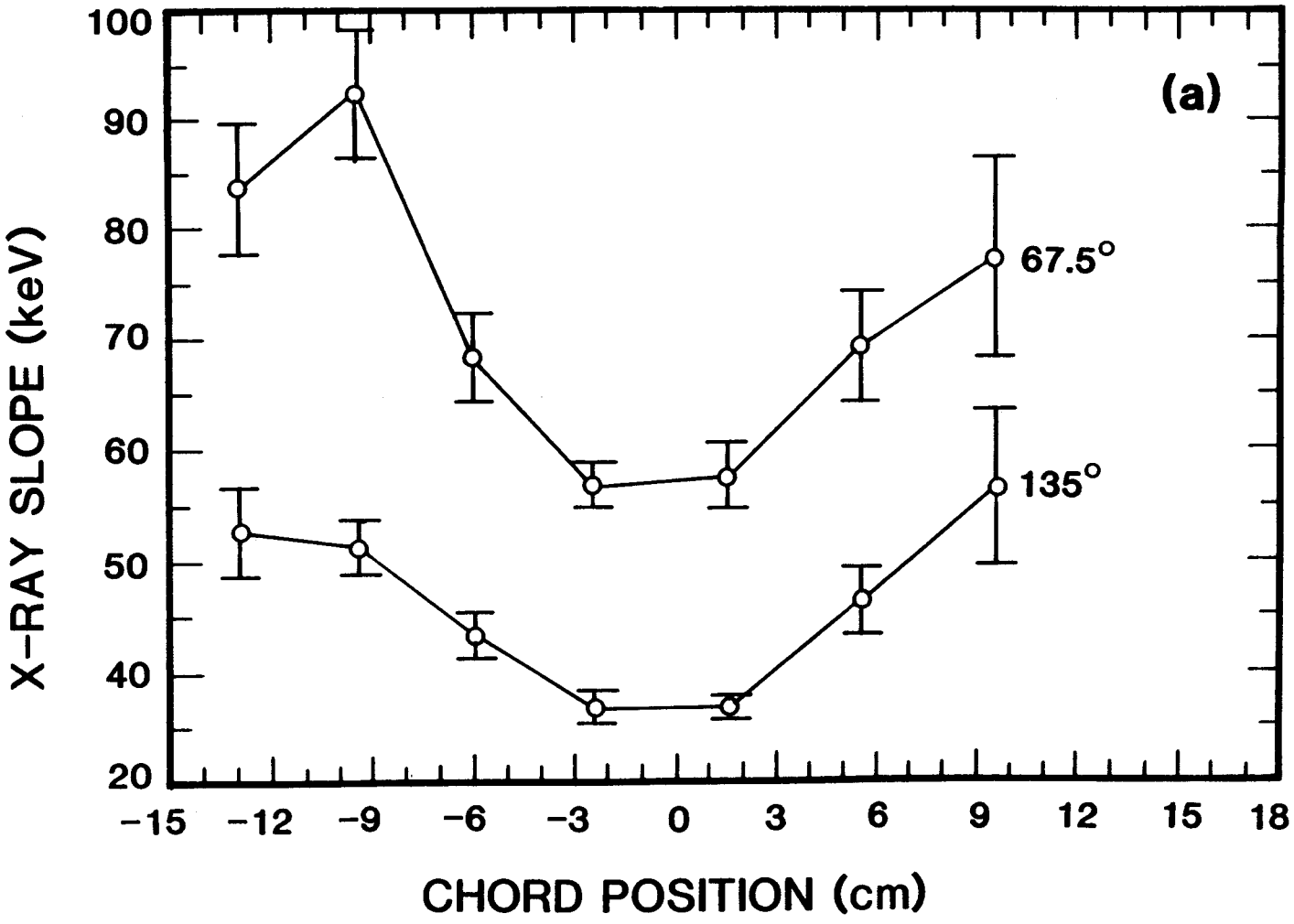
(a)
67.5°
135°
X-RAY SLOPE (keV)
100
90
80
70
60
50
40
20
-15
-12
-9
-6
-3
0
3
6
9
12
15
18
CHORD POSITION (cm)

Figure 7 (a)

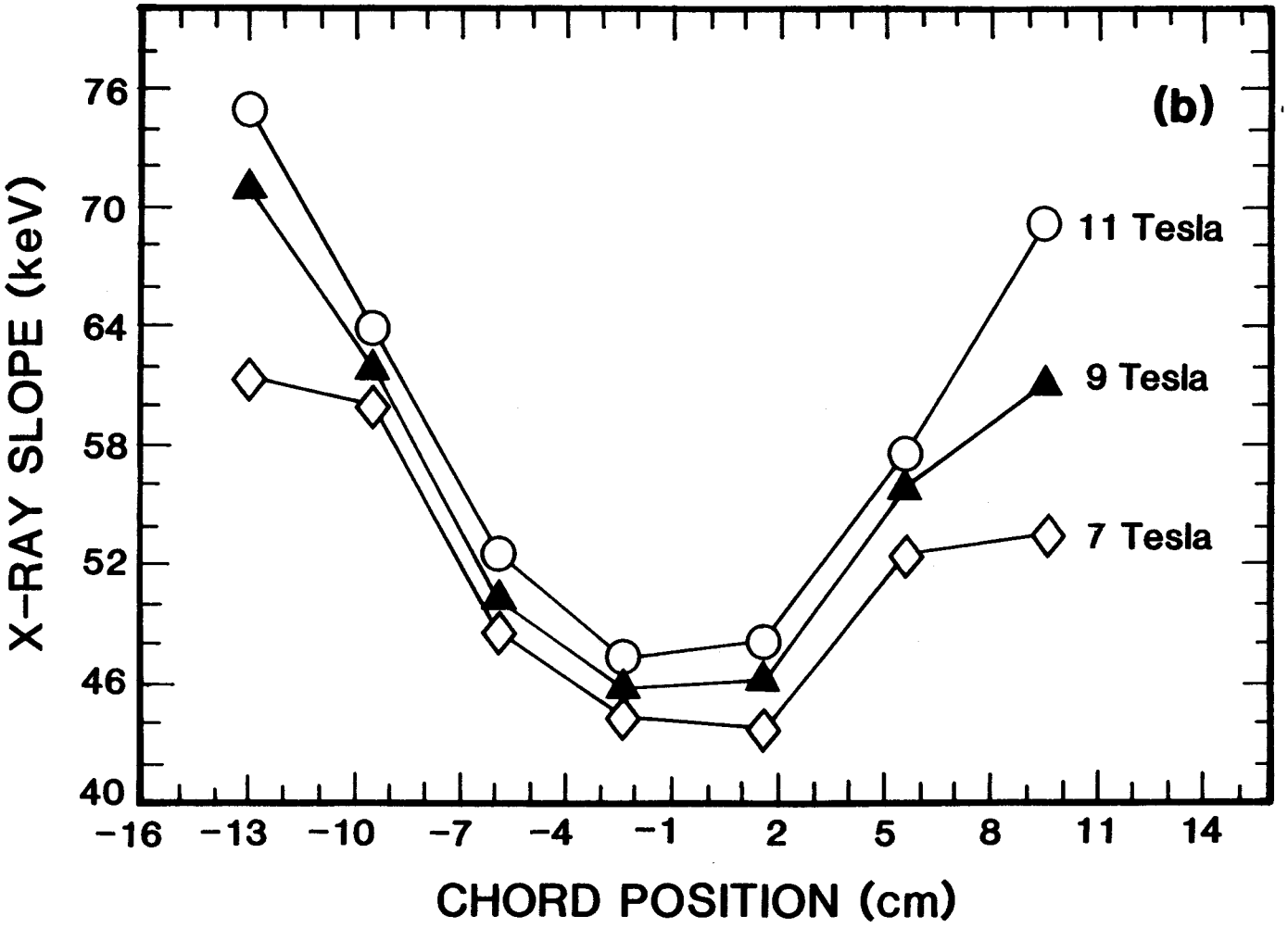
(b)
11 Tesla
9 Tesla
7 Tesla
X-RAY SLOPE (keV)
76
70
64
58
52
46
40
-16
-13
-10
-7
-4
-1
2
5
8
11
14
CHORD POSITION (cm)

Figure 7 (b)

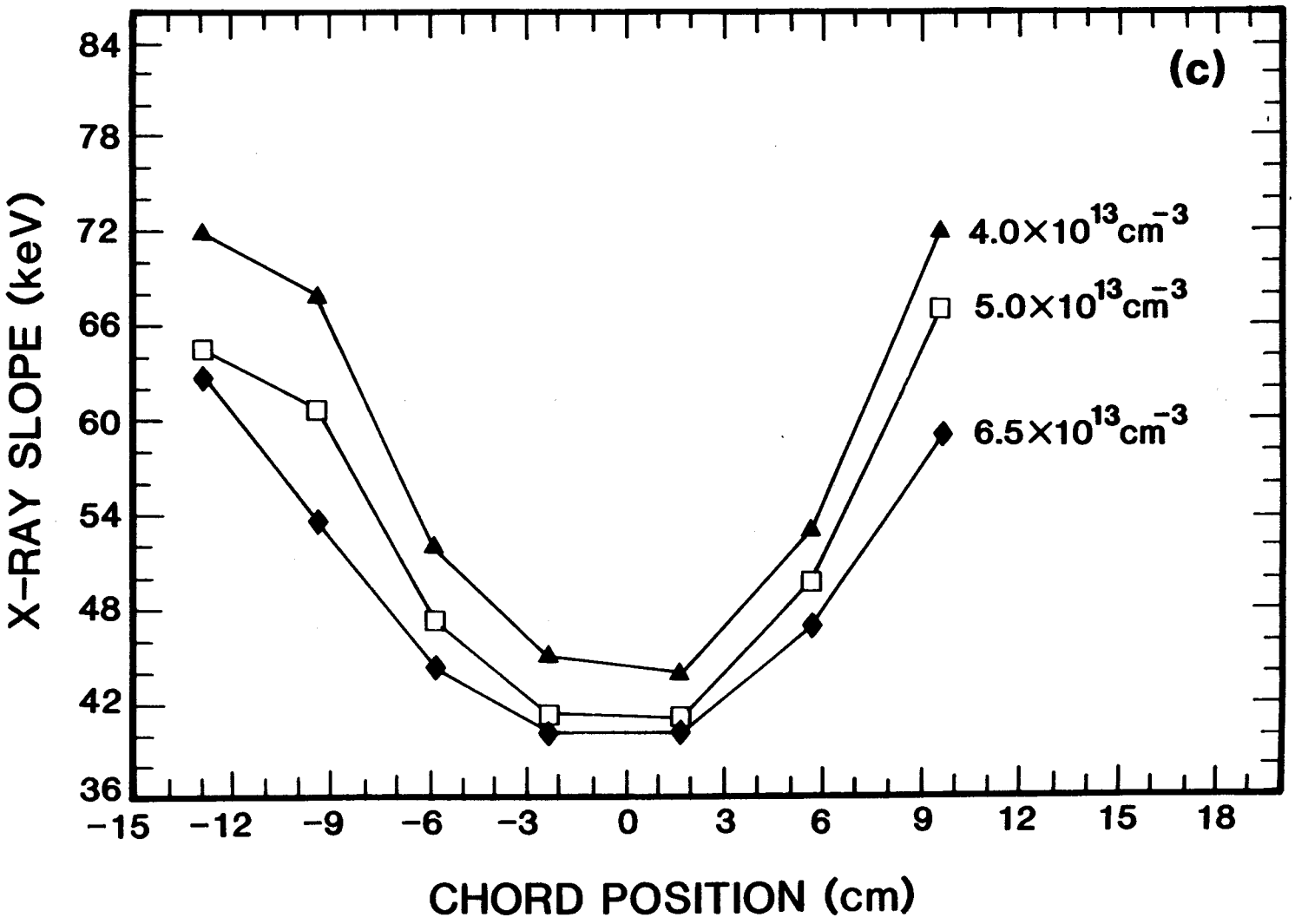
(c)
X-RAY SLOPE (keV)
84
78
72
66
60
54
48
42
36
-15
-12
-9
-6
-3
0
3
6
9
12
15
18
CHORD POSITION (cm)
4.0×10^13cm^-3
5.0×10^13cm^-3
6.5×10^13cm^-3

Figure 7 (c)

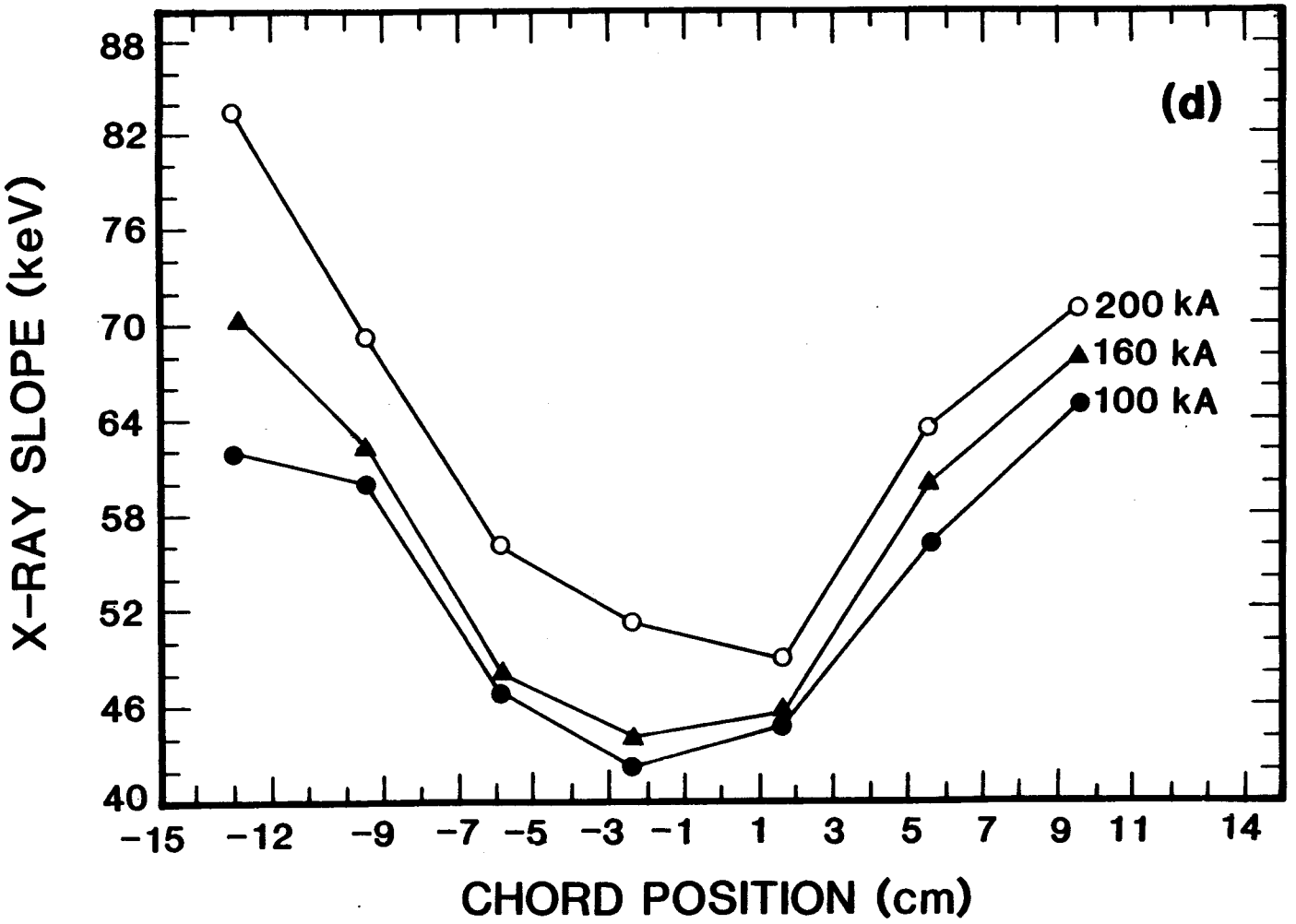
(d)
X-RAY SLOPE (keV)
88
82
76
70
64
58
52
46
40
-15
-12
-9
-7
-5
-3
-1
1
3
5
7
9
11
14
CHORD POSITION (cm)
200 kA
160 kA
100 kA

Figure 7 (d)

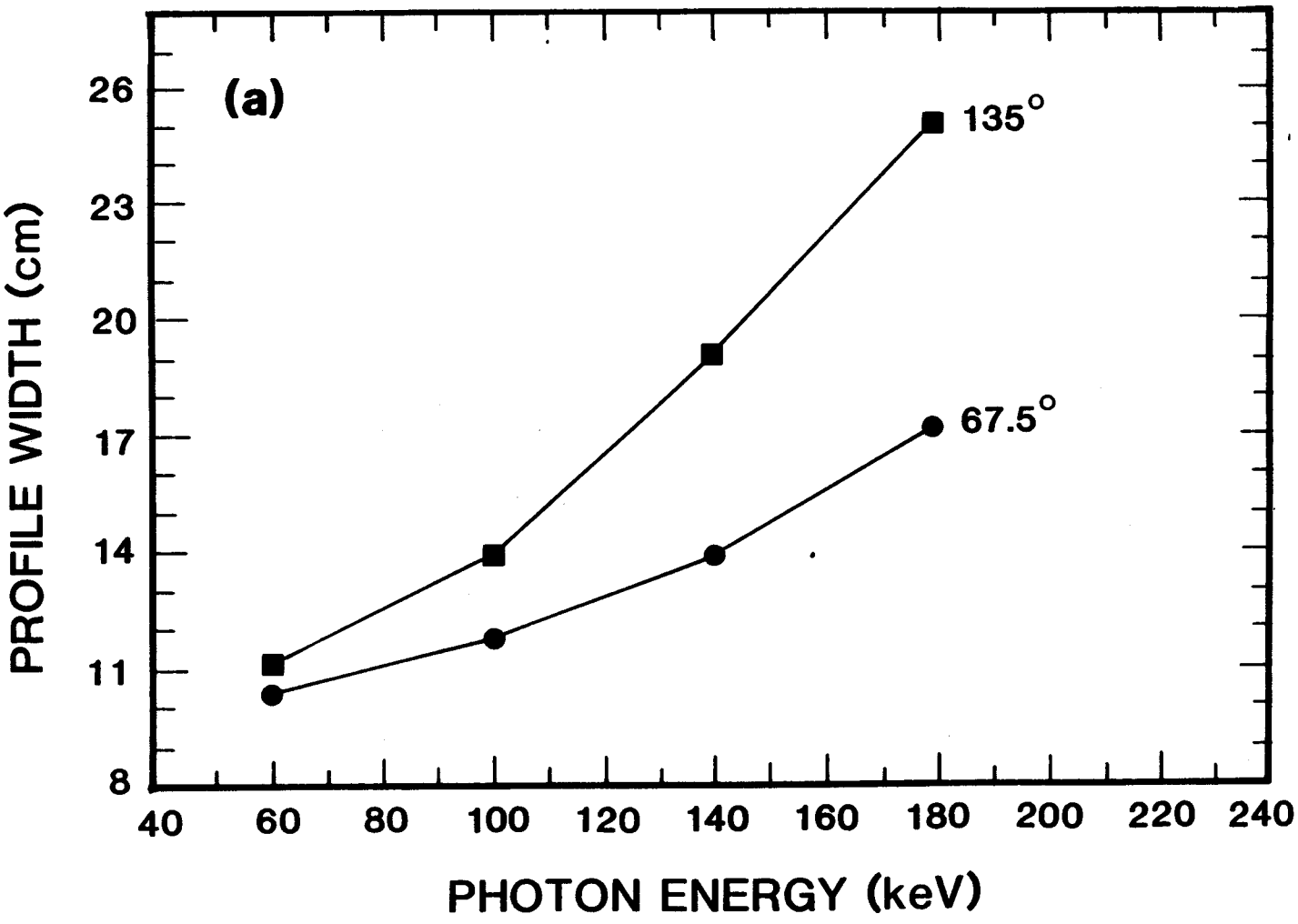
(a)
135°
67.5°
PROFILE WIDTH (cm)
26
23
20
17
14
11
8
40
60
80
100
120
140
160
180
200
220
240
PHOTON ENERGY (keV)

Figure 8 (a)

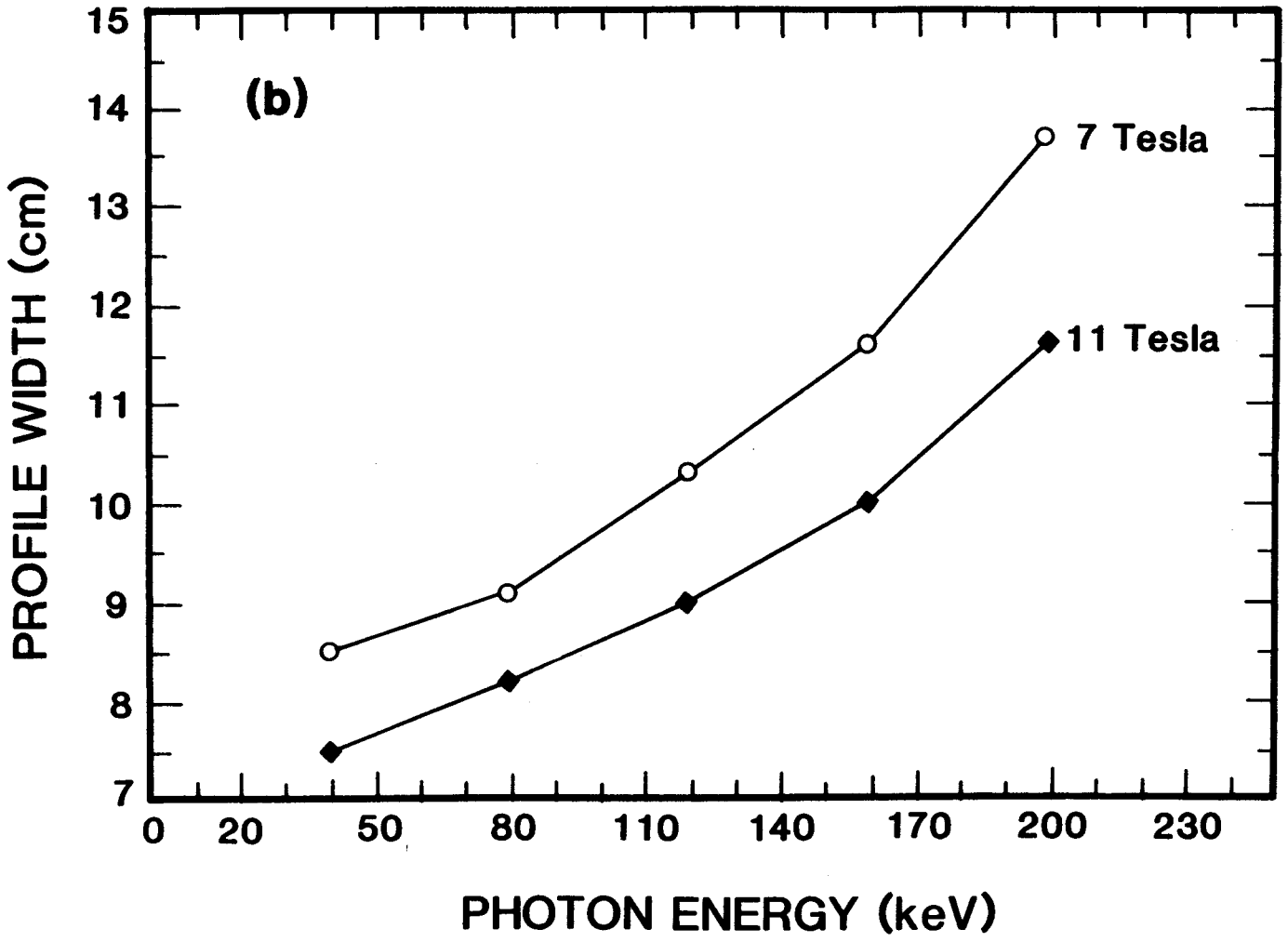
(b)
7 Tesla
11 Tesla
PROFILE WIDTH (cm)
PHOTON ENERGY (keV)
15
14
13
12
11
10
9
8
7
0
20
50
80
110
140
170
200
230

Figure 8 (b)

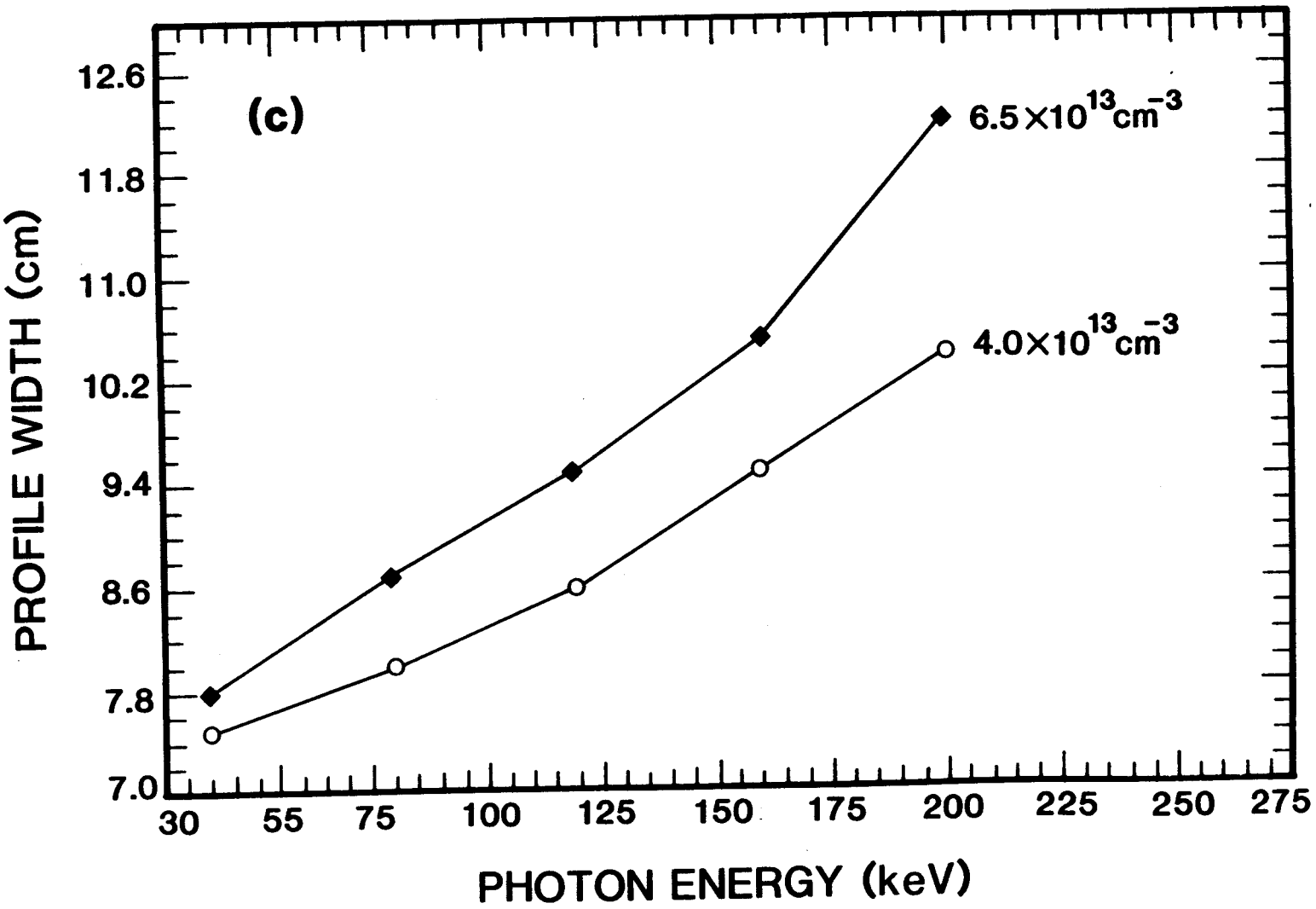
(c)
6.5×10^13cm^-3
4.0×10^13cm^-3
PROFILE WIDTH (cm)
12.6
11.8
11.0
10.2
9.4
8.6
7.8
7.0
30
55
75
100
125
150
175
200
225
250
275
PHOTON ENERGY (keV)

Figure 8 (c)

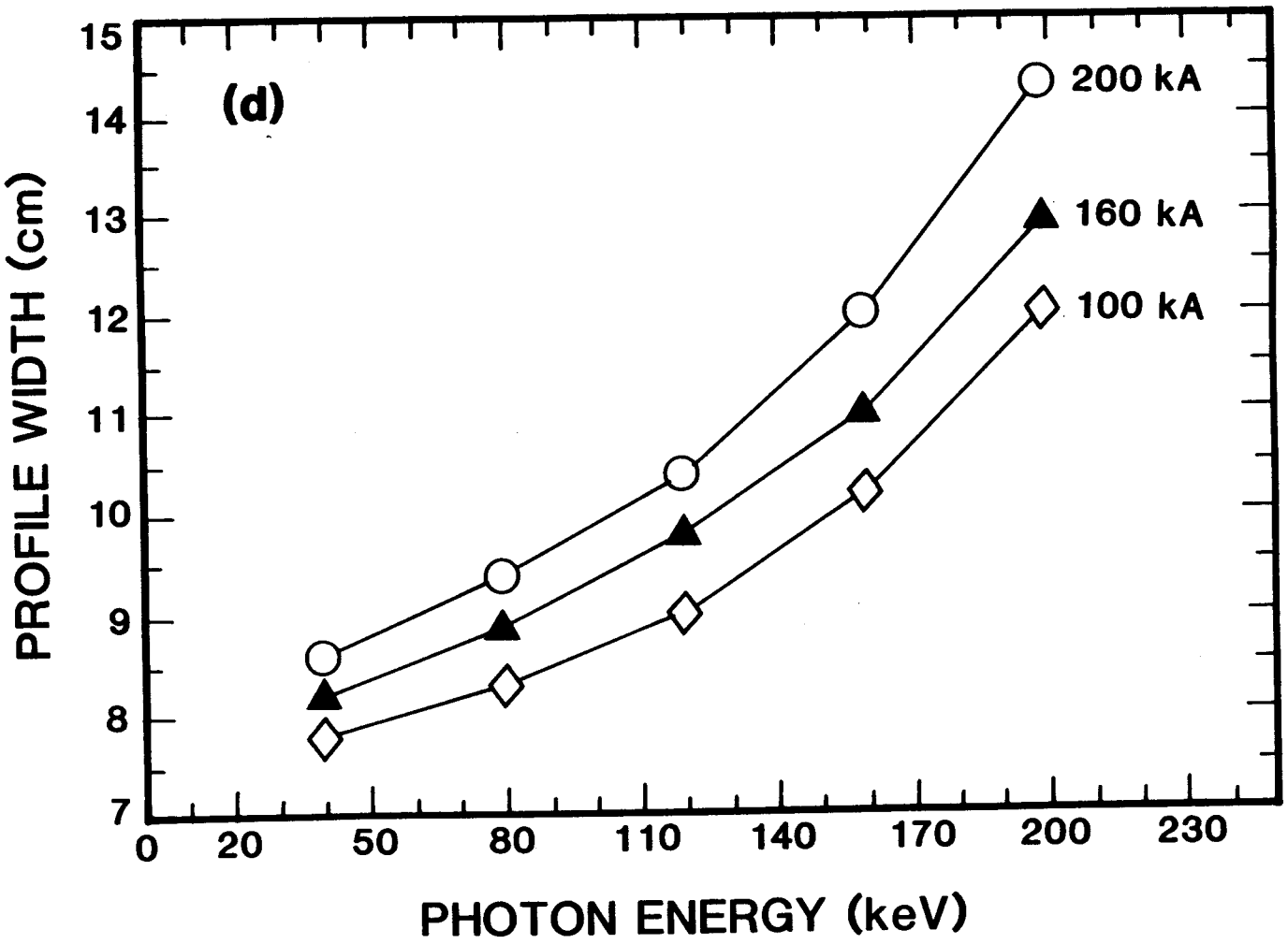
(d)
200 kA
160 kA
100 kA
PROFILE WIDTH (cm)
PHOTON ENERGY (keV)
15
14
13
12
11
10
9
8
7
0
20
50
80
110
140
170
200
230

Figure 8 (d)

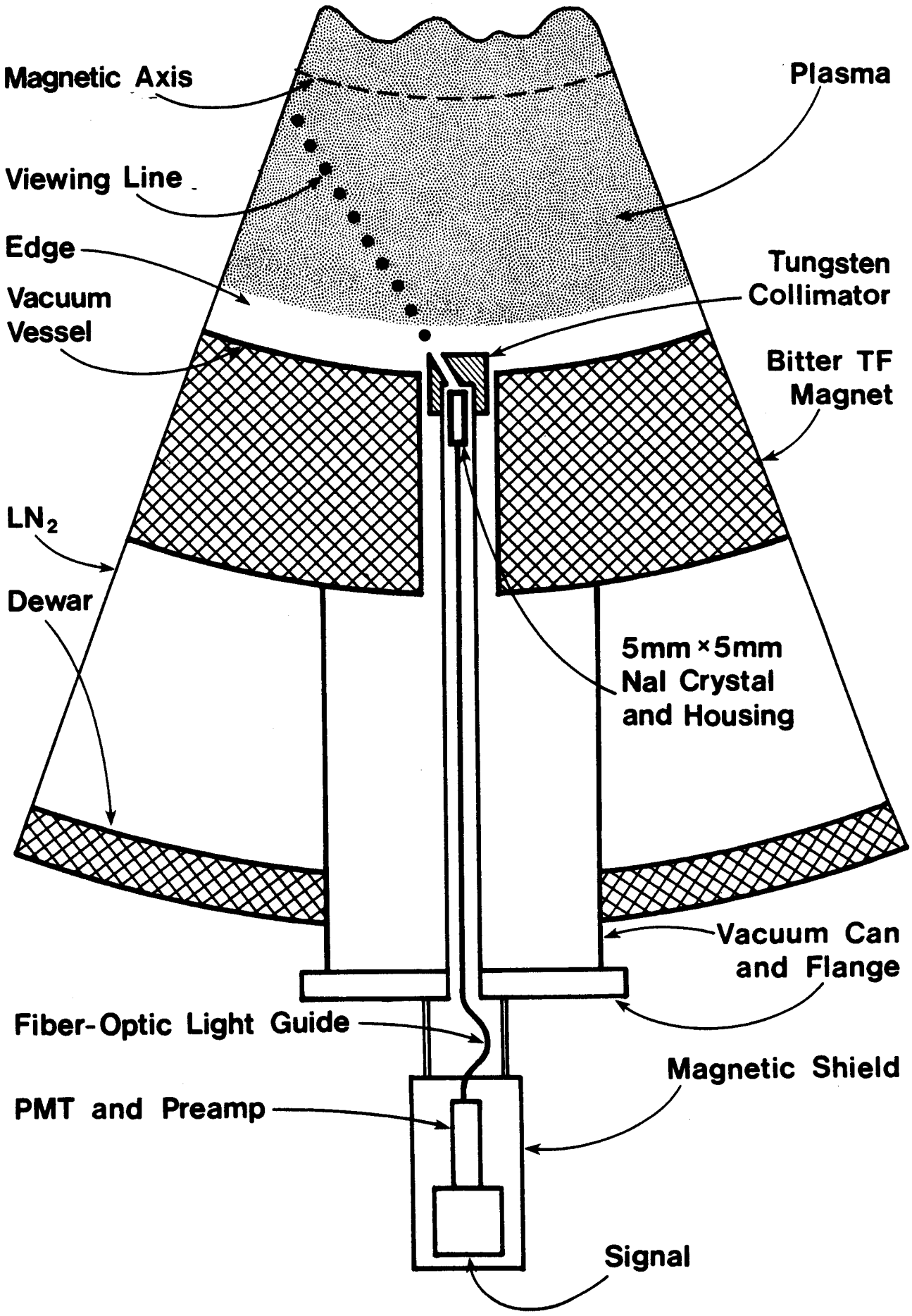
Magnetic Axis
Plasma
Viewing Line
Edge
Tungsten Collimator
Vacuum Vessel
Bitter TF Magnet
LN_2
Dewar
5mm×5mm NaI Crystal and Housing
Vacuum Can and Flange
Fiber-Optic Light Guide
Magnetic Shield
PMT and Preamp
Signal

Figure 9

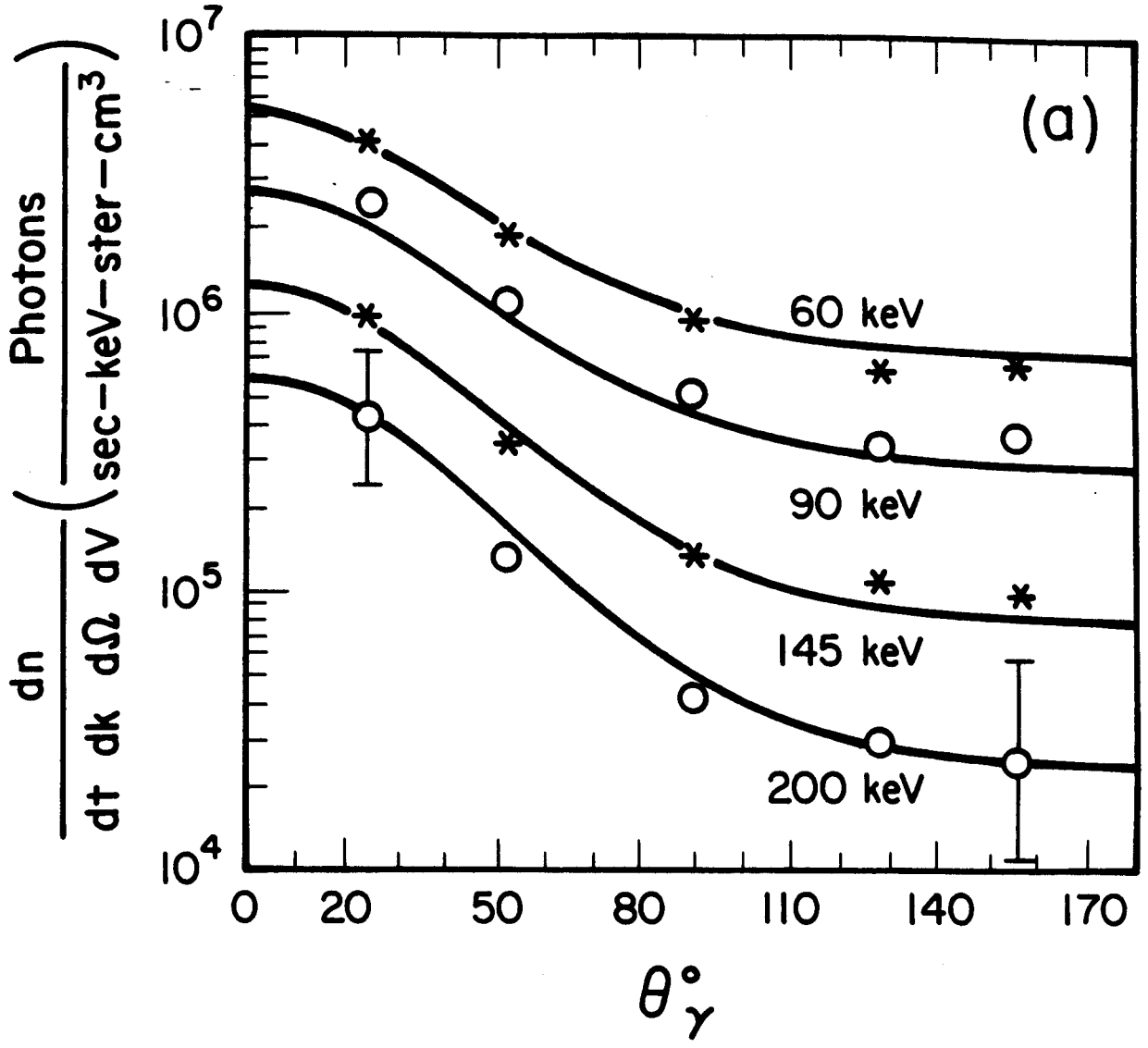
(a)
$\frac{dn}{dt\ dk\ d\Omega\ dV}\left(\frac{\text{Photons}}{\text{sec-keV-ster-cm}^3}\right)$
10^7
10^6
10^5
10^4
60 keV
90 keV
145 keV
200 keV
0
20
50
80
110
140
170
θ°_γ

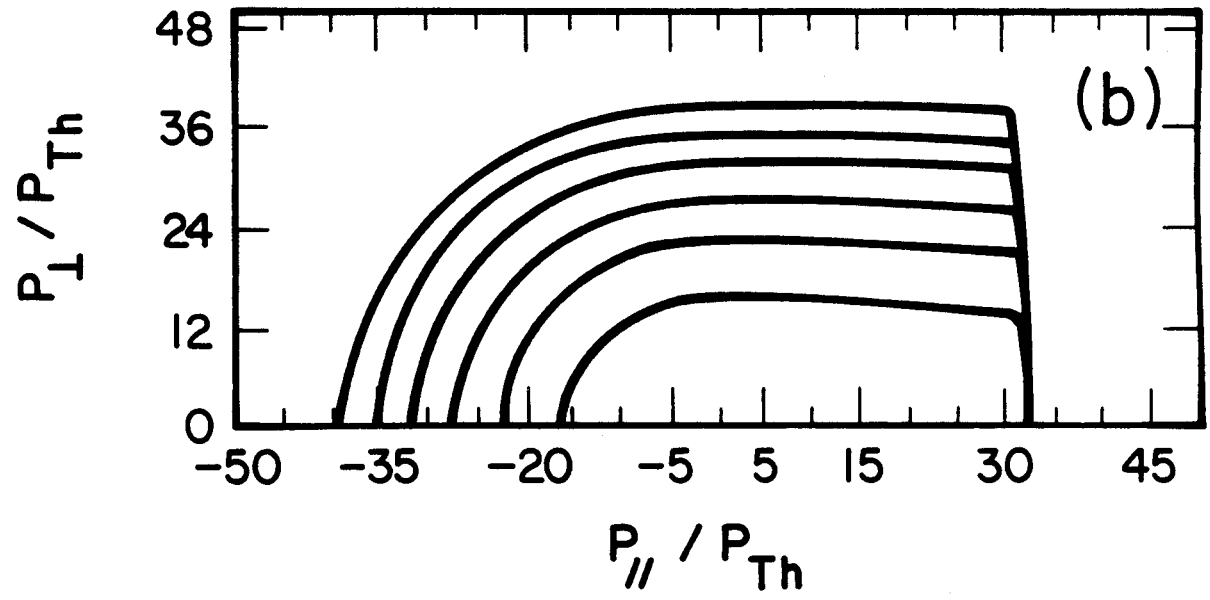
(b)
$P_\perp / P_{Th}$
48
36
24
12
0
−50
−35
−20
−5
5
15
30
45
$P_{//} / P_{Th}$

Figure 10

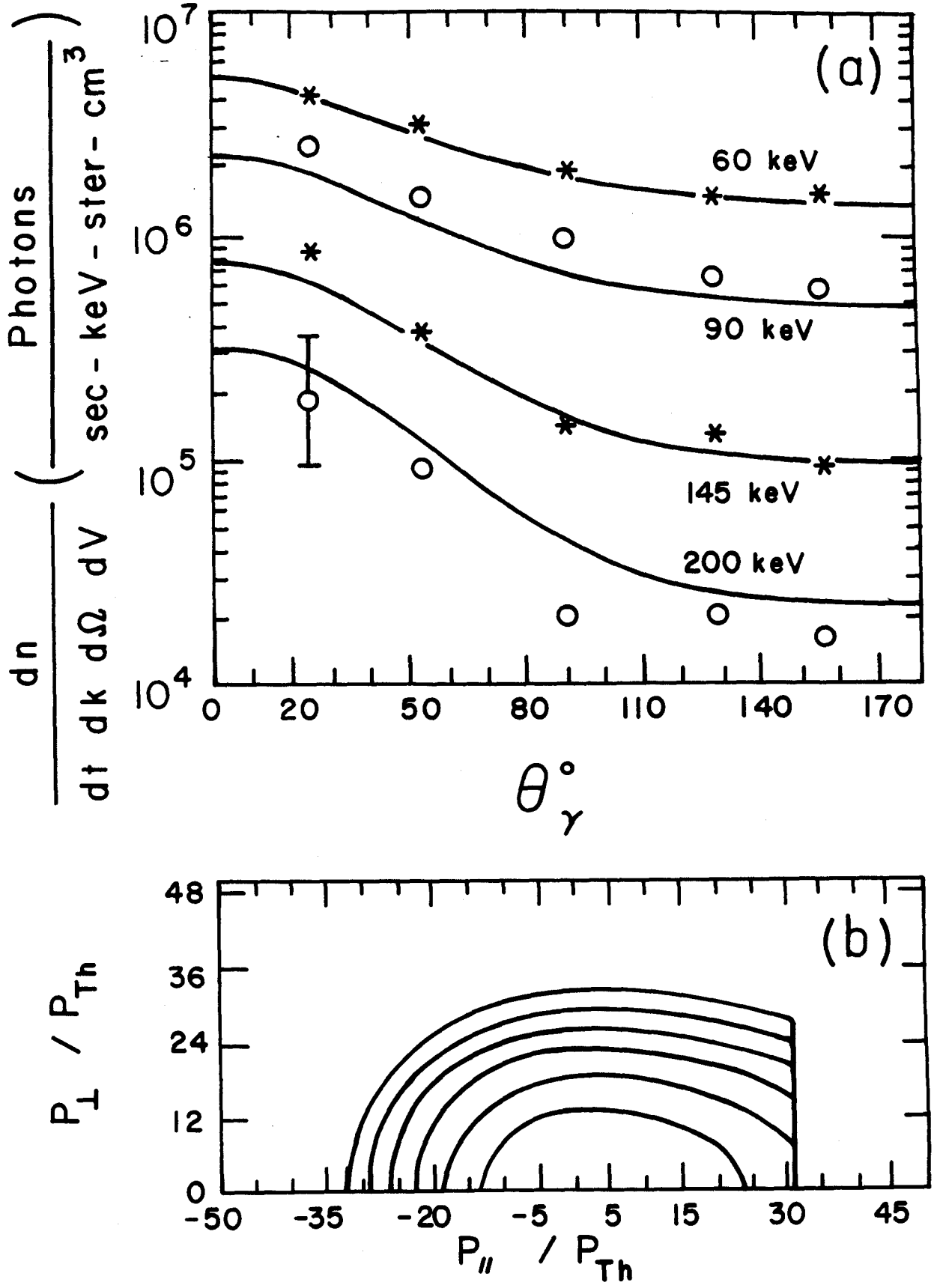
(a)
60 keV
90 keV
145 keV
200 keV
10^7
10^6
10^5
10^4
0
20
50
80
110
140
170
θ°_γ
$\frac{dn}{dt\ dk\ d\Omega\ dV}$ (Photons / sec - keV - ster - cm^3)
(b)
48
36
24
12
0
-50
-35
-20
-5
5
15
30
45
$P_\perp / P_{Th}$
$P_{//} / P_{Th}$

Figure 11